https://doi.org/10.5194/acp-2020-1279
Preprint. Discussion started: 12 January 2021

Atmospheric Chemistry and Physics Discussions

Isotopic constraints on atmospheric sulfate formation pathways in the Mt. Everest region, southern Tibetan Plateau

Kun Wang[1,2,8], Shohei Hattori[2], Mang Lin[2,3,11], Sakiko Ishino[2,4], Becky Alexander[5], Kazuki Kamezaki[2,10], Naohiro Yoshida[2,7,9], Shichang Kang[1,6,8]

[1]State Key Laboratory of Cryospheric Science, Northwest Institute of Eco-Environment and Resources, Chinese Academy of Sciences (CAS), Lanzhou 730000, China
[2]Department of Chemical Science and Engineering, School of Materials and Chemical Technology, Tokyo Institute of Technology, 4259 Nagatsuta-cho, Midori-ku, Yokohama, Kanagawa 226-8502, Japan
[3]State Key Laboratory of Isotope Geochemistry, Guangzhou Institute of Geochemistry, CAS, Guangzhou 510640, China
[4]National Institute of Polar Research, Research Organization of Information and Systems, Tokyo 190-8518, Japan
[5]Department of Atmospheric Sciences, University of Washington, Seattle, WA 98195, USA
[6]CAS Center for Excellence in Tibetan Plateau Earth Sciences, Beijing 100101, China
[7]Earth-Life Science Institute, Tokyo Institute of Technology, Meguro-ku, Tokyo 152-8551, Japan
[8]University of Chinese Academy of Sciences, Beijing 100049, China
[9]National Institute of Information and Communications Technology, Koganei, Tokyo 184-8795, Japan
[10]Faculty of Science and Technology, Sophia University, 7-1 Kioi-cho, Chiyoda-ku, Tokyo, 102-8554, Japan
[11]CAS Center for Excellence in Deep Earth Science, Guangzhou 510640, China

Correspondence to: Shichang Kang (shichang.kang@lzb.ac.cn) and Shohei Hattori (hattori.s.ab@m.titech.ac.jp)

Abstract. As an important atmosphere constituent, sulfate aerosols exert profound impacts on climate, ecological environment, and human health. The Tibetan Plateau (TP), identified as the 'Third Pole', contains the largest land ice masses outside the poles and has attracted wide attention on its environment and climatic change. However, the mechanisms of sulfate formation in this specific region remain poorly characterized. Oxygen-17 anomaly ($\Delta^{17}O$) has been used as a probe to constrain the relative importance of different pathways leading to sulfate formation. Here, we report the $\Delta^{17}O$ values in atmospheric sulfate collected at a remote site in the Mt. Everest region to decipher the possible formation mechanisms of sulfate in such a pristine environment. Throughout the sampling campaign (April-September 2018), the $\Delta^{17}O$ in non-dust sulfate show an average of 1.7 ± 0.5‰ which is higher than most existing data in modern atmospheric sulfate. The seasonality of $\Delta^{17}O$ in non-dust sulfate exhibits high values in the pre-monsoon and low values in the monsoon, opposite to the seasonality in $\Delta^{17}O$ for both sulfate and nitrate (i.e., minima in warm season and maxima in cold season) observed from diverse geographic sites. This high $\Delta^{17}O$ in non-dust sulfate found in this region clearly indicates the important role of the S(IV) + O_3 pathway in atmospheric sulfate formation promoted by high cloud water pH condition. Overall, our study provides an observational constraint on atmospheric acidity in altering sulfate formation pathways particularly in dust-rich environments, and such identification of key processes provides an important basis for a better understanding of the sulfur cycle in the TP.

https://doi.org/10.5194/acp-2020-1279
Preprint. Discussion started: 12 January 2021

Atmospheric Chemistry and Physics Discussions

1 Introduction

As a predominant chemical component of atmospheric aerosols, sulfate (SO_4^{2-}) plays an important climatic role as it tend to make clouds more reflective and increases their lifetimes, thereby causing a net cooling effect on the planet (Charlson et al., 1992; Kulmala et al., 2000). Furthermore, it is also a major source of acidity in aerosols and cloud water, and is implicated in acid deposition that exerts adverse effects on ecological environment and human health (Chang et al., 1987). Sulfate is mainly produced within the atmosphere by the oxidation of sulfur dioxide (SO_2), which is largely emitted from combustion processes (e.g., fossil fuel and biomass combustion) and volcanoes, and is also generated by oxidation of other sulfur-containing species such as dimethyl sulfide (DMS) emitted by oceanic phytoplankton. The conversion of SO_2 to sulfate is mainly dominated by gas- and aqueous-phase oxidation of SO_2 by various oxidants (Liang and Jacobson, 1999; Mchenry and Dennis, 1994; Savarino et al., 2000; Lee and Thiemens, 2001; Stockwell and Calvert, 1983; Schwartz, 1987). In the gas-phase, SO_2 is mainly oxidized by hydroxyl radical (OH) to produce sulfuric acid (H_2SO_4) that can nucleate new particles, and increase aerosol number density and the population of cloud condensation nuclei (Kulmala et al., 2000). Aqueous-phase sulfate formation involves dissolution of SO_2 followed by dissociation of $SO_2{\cdot}H_2O$ to HSO_3^- and SO_3^{2-}. The total dissolved sulfur in solution, referred to as S(IV) due to their oxidation state of 4, is the sum of $SO_2{\cdot}H_2O + HSO_3^- + SO_3^{2-}$, which can be oxidized to sulfate via multiple pathways, mainly including oxidation by O_3, H_2O_2, and O_2 catalyzed by transition metals ions (TMIs, Fe^{3+} and Mn^{2+}). Note that S(IV) can also be oxidized in the aqueous phase by other oxidants including NO_2 (Lee and Schwartz, 1983), NO_3 (Feingold et al., 2002), and HNO_4 (Dentener et al., 2002), but these are not thought to be significant on the global scale. Hypohalous acids (HOCl and HOBr) were proposed to be the potentially important oxidants only in the marine boundary layer (Vogt et al., 1996; Chen et al., 2016). Sulfate produced in the aqueous phase does not lead to nucleation of new particles, but can increase particle growth rates since it forms on an existing particles (Kaufman and Tanre, 1994). In addition, different aqueous pathways would be also responsible for different aerosol radiative forcing effects (Harris et al., 2013), and thus, a detailed understanding of partitioning between the major oxidation pathways is critical for accurate estimation of the magnitude and spatial distribution of sulfate aerosol cooling in assessments of current and future climate. Despite the recent progress, the formation mechanisms of atmospheric sulfate still remain to be elucidated, especially for some specific regions with complex ambient conditions.

The Tibetan Plateau (hereafter referred to as TP), covering an area of ~2.5×10^6 km^2 and having an average elevation of over 4000 m above sea level (a.s.l.), has been known as the 'Third Pole' (Kang et al., 2010). It contains the largest land ice masses outside the poles and supplies water for more than one billion people (Immerzeel et al., 2010). As one of the most sensitive areas to global change (Liu and Chen, 2000) and adjacent to the world's most polluted areas, i.e., South and East Asia, the TP region has attracted wide attention on its environmental and climatic impacts. Kang et al. (2019) summarized that the exogenous air pollutants can enter into the TP's environments via long-range transport, with regional impacts such as accelerating snow/glacier melting and degrading water quality. As one of those pollutants, atmospheric sulfate can affect not only aquatic/terrestrial ecosystems but also radiative forcing in the TP region. One recent study revealed that the human induced increase of atmospheric sulfate concentrations might be responsible for the persistent weakening of temperature

https://doi.org/10.5194/acp-2020-1279
Preprint. Discussion started: 12 January 2021

Atmospheric Chemistry and Physics Discussions

seasonality over the TP since the 1870s (Duan et al., 2017). Correspondingly, a deep understanding of the formation mechanisms of sulfate in this region is crucial for an accurate assessment of the environmental impacts as well as cryospheric extent variation in the TP region.

The mass-independent oxygen-17 anomaly ($\Delta^{17}O$) is any deviation from the linear approximation of $\delta^{17}O = 0.52 \times \delta^{18}O$, a relationship that describes the mass-dependent process, and can be quantified as $\Delta^{17}O = \delta^{17}O - 0.52 \times \delta^{18}O$ (Thiemens, 1999), wherein $\delta^{17,18}O = [(^{17,18}O/^{16}O)_{sample}/(^{17,18}O/^{16}O)_{VSMOW} - 1]$. Since it was discovered to be produced during the chemical formation of ozone (O_3) for the first time in 1980s, (Thiemens and Heidenreich, 1983), the $\Delta^{17}O$ has been studied extensively and proven to be a powerful tool in discerning the formation mechanisms of atmospheric sulfate (e.g., Ishino et al., 2017; Alexander et al., 2002, 2005, 2009, 2012; Li et al., 2013; Jenkins and Bao, 2006; He et al., 2018; McCabe et al., 2006; Lee and Thiemens, 2001; Dominguez et al., 2008; Walters et al., 2019; Lin et al., 2017; Lin et al., 2020). Because the oxidants transfer unique $\Delta^{17}O$ signal to the produced sulfate (Savarino et al., 2000), $\Delta^{17}O$ in sulfate ($\Delta^{17}O(SO_4^{2-})$) reflects the relative importance of various oxidation pathways involved in its formation. Once emitted, SO_2 quickly exchanges its oxygen atoms with abundant water vapor ($\Delta^{17}O$ = 0‰) in the atmosphere (Lyons, 2001), and any source signature in the oxygen isotopes is erased (Holt et al., 1981). Thus, unlike $\delta^{18}O$ values that integrate both the $\delta^{18}O$ values of reactants (SO_2 and oxidants) and oxygen isotopic kinetic and/or equilibrium fractionation effects during the oxidation processes, atmospheric transport and deposition, $\Delta^{17}O$ is fairly insensitive to mass-dependent fractionations and solely depend on the oxidation pathway of SO_2 to sulfate, which render $\Delta^{17}O$ a powerful tool to investigate the formation processes of sulfate. Laboratory experiments demonstrated that the mass-independent sulfate in the troposphere mainly originates from oxygen atom transfer from O_3 ($\Delta^{17}O$ = 25.6 ± 1.3 ‰ for bulk tropospheric O_3 (Ishino et al., 2017; Savarino et al., 2000; Vicars and Savarino, 2014)) and H_2O_2 ($\Delta^{17}O$ = 1.6 ± 0.3 ‰ (Savarino and Thiemens, 1999) during oxidation of SO_2, while oxidation by OH ($\Delta^{17}O$ = 0‰) as well as TMI-catalyzed oxidation by O_2 ($\Delta^{17}O \approx -0.3$‰) produce sulfate with $\Delta^{17}O$ at or near 0‰ (Vicars and Savarino, 2014; Savarino et al., 2000; Lyons, 2001). Based on the transfer of the $\Delta^{17}O$ signature from the oxidant to the produced sulfate (Savarino et al., 2000), $\Delta^{17}O$ values of sulfate formed via the main oxidation pathways are as follows:

$$SO_2 + OH \rightarrow \Delta^{17}O(SO_4^{2-}) = 0‰ \quad (1)$$

$$S(IV) + O_3 \rightarrow \Delta^{17}O(SO_4^{2-}) = 6.5 \pm 0.3‰ \quad (2)$$

$$S(IV) + H_2O_2 \rightarrow \Delta^{17}O(SO_4^{2-}) = 0.8 \pm 0.2‰ \quad (3)$$

$$S(IV) + O_2 \rightarrow \Delta^{17}O(SO_4^{2-}) = -0.1‰ \quad (4)$$

S(IV) oxidation by other oxidants (e.g., NO_2 and hypohalous acids) is expected to produce sulfate with $\Delta^{17}O$ near 0‰ as described in He et al. (2018) and Chen et al. (2016). Besides, the primary sulfate, including natural (mineral dust and sea salt) and anthropogenic (e.g., fossil fuel combustion) sources, also possesses a $\Delta^{17}O$ value of 0‰ (Dominguez et al., 2008; Lee and Thiemens, 2001). As a non-labile oxyanion, once produced, sulfate in the atmosphere does not undergo further oxygen isotope exchange with ambient species. Theoretically, $\Delta^{17}O(SO_4^{2-})$ values in the real atmosphere can be predicted using the estimated

https://doi.org/10.5194/acp-2020-1279
Preprint. Discussion started: 12 January 2021

Atmospheric Chemistry and Physics Discussions

fractional contribution of each formation pathway and corresponding $\Delta^{17}O$ values by atmospheric chemical transport models (e.g., McCabe et al., 2006; Sofen et al., 2011). By comparing *in-situ* observations with modeling results, the missing processes involved in sulfate formation can be quantified. However, existing observations of $\Delta^{17}O(SO_4^{2-})$ values provide sparse spatial coverage, particularly in remote regions such as the TP.

Although the TP is one of the most climatically important regions in the world, until now there are almost no observational studies focusing on the mechanisms of sulfate formation in this region, which partly due to the harsh environmental conditions. Here, for the first time, we present relatively long term $\Delta^{17}O$ observations in atmospheric sulfate in this region, which is an important addition to the global sulfate isotope dataset. Using the APCC (Atmospheric Pollution and Cryospheric Changes) monitoring network (Kang et al., 2019), aerosols samples (total suspended particulates, TSP) were collected from a remote site located in the northern slope of Mt. Everest (27.98°N, 86.92°E; 8844.43 m a.s.l.) from April to September 2018. Located at the boundary of the Indian Monsoon and the southern edge of the TP, the Mt. Everest region is a possible receptor of atmospheric pollutants transported directly from the Indian subcontinent to the TP. By characterizing the observed $\Delta^{17}O$ data combined with model simulations (GEOS-Chem global three-dimensional atmospheric chemical transport model), we decipher the possible mechanisms of sulfate formation in the Mt. Everest region, with important implications for the sulfur cycle, atmospheric oxidation processes and models of climatic change in the TP region.

2 Materials and Methods

2.1 Observation site and aerosol sampling

The field sampling was conducted at the Qomolangma Station for Atmospheric and Environmental Observation and Research, Chinese Academy of Sciences (QOMS; 28.36°N, 86.95°E; 4300 m a.s.l.) (Fig. 1). The sampling site has been previously described in detail (e.g., Ma et al., 2011). In brief, the QOMS is located in an S-shaped valley (Fig. 1b) where the surface is covered by sandy soil with sparse vegetation and gravel, and the surrounding region has limited human activity. Almost all precipitation occurs during the monsoon season, and temperature and relative humidity (RH) also show clear seasonal patterns with higher values in the monsoon season than in the non-monsoon seasons (Fig. 1c). According to the measured meteorological parameters, mainly precipitation, the entire year of 2018 in the Mt. Everest region can be divided into four seasons, i.e., pre-monsoon (March to May), monsoon (June to August), post-monsoon (September to November), and winter (December to February).

The TSP samples were collected by a high-volume air sampler (Laoying-2031, LAOYING Institute, China) mounted on the roof of an instrument room (Fig. 1d). Each sample was collected on a pre-baked (450 °C for 4 h) quartz filters (Whatman Inc., UK), and covered 4-7 d at a flow rate of 1.05 m^3 min^{-1}. After sampling, the filters were preserved properly (wrapped using aluminum foil, sealed in polyethylene bags and stored in a clean refrigerator at –20 °C), and eventually shipped to Tokyo Institute of Technology, Japan for further chemical and isotopic analyses. A filter was subjected to the same chemical analyses

https://doi.org/10.5194/acp-2020-1279
Preprint. Discussion started: 12 January 2021

Atmospheric Chemistry and Physics Discussions

but without turning pump on when sampling for blank test. A few samples with insufficient amount of sulfate were combined with adjacent samples to obtain enough sulfates to run isotopic measurements.

2.2 Chemical and isotopic analyses

A detailed description of the method for chemical analysis of water-soluble inorganic ions can be found in Wang et al. (2020a). Briefly, a small portion of each filter was soaked in 30 mL of deionized water in a 50 mL centrifuge tube under ultrasonic conditions for 20 min. Then the sample solution was separated from insoluble materials and the filter by a centrifugal filter unit centrifuged for 10 min. This method can recover more than 98% of the initial water volume. The major anions (e.g., SO_4^{2-} and NO_3^-) were quantified by an ion chromatography (Dionex ICS-2100, Thermo Fisher Scientific) while the cations (e.g., Ca^{2+} and K^+) were detected by another ion chromatography (881 Compact IC pro, Metrohm). The uncertainty of both instruments was approximately 4% as determined by repeated measurements of standards. The reported concentrations of ions in this study are corrected by a measured field blank.

Organic material, which may reduce the precision and accuracy of oxygen isotopic measurements, was removed by applying a high-temperature heating method (Xie et al., 2016). Briefly, the sample precipitates were heated at 450 °C for 2 h prior to isotopic measurements, and the organic materials were largely removed as detected by the ion chromatography. As demonstrated by Xie et al. (2016), the effect of oxygen isotopic exchange during the heating is negligible. After the removal of organic materials, the oxygen isotopic compositions of sulfate were measured using a pyrolysis technique in a continuous flow system as introduced by Savarino et al. (2001) with further modifications described in several later studies (Geng et al., 2013; Schauer et al., 2012). Sulfate was firstly separated from other chemical impurities via ion chromatography (Dionex Integrion, Thermo Fisher Scientific). About 1 μmol of sulfate in acidic form was then chemically converted into sodium salt (Na_2SO_4) using a cation-exchange resin. 1 mL of H_2O_2 (30%) was then added to the Na_2SO_4 samples and dried in a vacuum centrifuge with the aim to remove any remaining organic materials. The re-dissolved Na_2SO_4 was subsequently converted into silver salt (Ag_2SO_4) by passing it through the cation-exchange resin that was in silver form. After being dried in the vacuum centrifuge, the Ag_2SO_4 powder contained in a custom-made quartz cup was thermally decomposed to O_2 and SO_2 at a temperature of 1000 °C. The gas products were carried by ultra-pure helium through a cleanup trap held at –196 °C to remove byproducts (mainly SO_2 and trace SO_3). The O_2 was then cryofocused by a liquid nitrogen trap with Molecular Sieve 5Å. After thawing, the released O_2 was further purified through a gas chromatography, and finally the obtained O_2 was carried into the isotope ratio mass spectrometer (MAT253, Thermo Fisher Scientific) for oxygen isotopic measurement. Since oxygen isotope ($\delta^{17}O$ and $\delta^{18}O$) exchange between the produced O_2 and quartz materials ($\Delta^{17}O$ = 0‰) occurring during the pyrolysis process shifts the $\Delta^{17}O$ values (Savarino et al., 2001; Schauer et al., 2012), the raw $\Delta^{17}O$ values were corrected by estimating the magnitude of the oxygen isotope exchange using inter-laboratory calibrated standards, as described in Ishino et al. (2017) and Gautier et al. (2019). Due to the unknown $\delta^{17}O$ and $\delta^{18}O$ values of each quartz material used in this study, it is difficult to get reliable corrected $\delta^{17}O$ and $\delta^{18}O$ values, thus we don't discuss these values in the following sections. The 1σ precision of

https://doi.org/10.5194/acp-2020-1279
Preprint. Discussion started: 12 January 2021


Atmospheric Chemistry and Physics Discussions

corrected $\Delta^{17}O$ was ± 0.1‰ based on replicate analyses (n = 20) of the standard B ($\Delta^{17}O(SO_4^{2-})$ = 2.4‰) with five independent runs of this study.

2.3 Model description

GEOS-Chem is a global 3-D model of atmospheric composition (www.geos-chem.org) originally developed by Bey et al. (2001). In this study, we use GEOS-Chem (version 12.5.0, DOI: 10.5281/zenodo.3403111) driven by assimilated meteorological fields from MERRA-2 reanalysis data product from NASA Global Modeling and Assimilation Office's GEOS-5 Data Assimilation System. We simulate aerosol-oxidant tropospheric chemistry containing detailed HO_X-NO_X-VOC-ozone-BrO_X chemistry (Bey et al., 2001; Pye et al., 2009; Sherwen et al., 2016). The model was run at 4° × 5° horizontal resolution and 47 vertical levels up to 0.01 hPa, and spun up for 1 year before each simulation. In the model, sulfate is produced from gas-phase oxidation of SO_2 by OH, aqueous-phase oxidation of S(IV) by H_2O_2, O_3, HOBr, metal-catalyzed O_2, and heterogeneous oxidation on sea-salt aerosols and dust aerosols by O_3 (Alexander et al., 2012; Chen et al., 2017; Fairlie et al., 2010). To examine the importance of sulfate formation on dust aerosol, we tested the model simulation with or without sulfate formation on mineral dust (Fairlie et al., 2007; 2010).

The parameterization of the metal-catalyzed S(IV) oxidation is described in Alexander et al. (2009). We consider Fe and Mn which catalyze S(IV) oxidation in the oxidation states of Fe(III) and Mn(II). Dust-derived Fe ($[Fe]_{dust}$) is scaled to the modeled dust concentration as 3.5% of total dust mass, and dust-derived Mn is a factor of 50 times lower than $[Fe]_{dust}$. Anthropogenic Fe ($[Fe]_{anthro}$) is scaled as 1/30 of primary sulfate and anthropogenic Mn ($[Mn]_{anthro}$) is 10 times lower than that of $[Fe]_{anthro}$. In the model, 50% of Mn is dissolved in cloud water as Mn(II) oxidation state, and 10% of $[Fe]_{dust}$ and 1% of $[Fe]_{anthro}$ are dissolved in cloud water as Fe(III) oxidation states.

For pH-dependent S(IV) partitioning, bulk cloud water pH is calculated as described in Alexander et al. (2012). We use the parameterization as described in Yuen et al. (1996) to account for the effect of heterogeneity of cloud water pH on S(IV) partitioning and subsequent aqueous phase sulfate formation (Alexander et al., 2012). Sulfate formed from each oxidation pathway was treated as a different "tracer" in the model as described elsewhere (Chen et al., 2016; Sofen et al., 2011).

For anthropogenic emissions, we use the Community Emissions Data System (CEDS) inventory (http://www.globalchange.umd.edu/ceds/) (Hoesly et al., 2018). Emission species for CEDS include aerosol (black carbon (BC), organic carbon (OC)), aerosol precursors, and reactive compounds (SO_2, NO_X, NH_3, CO, non-methane volatile organic carbon (NMVOC)). We use the biomass burning emissions from the CMIP6 (BB4CMIP) inventory for each individual year (Van Marle et al., 2017). Emission species for BB4CMIP include the following species: BC, CH_4, CO, NH_3, NMVOC, NO_X, OC, SO_2, and HCl. We prescribe latitudinal CH_4 concentrations for historical simulations. CH_4 concentrations are based on NOAA GMD flask observations (www.esrl.noaa.gov/gmd/ccgg/trends_ch4/).

Model simulations were performed for the year 2013. In addition to the model with calculated cloud water pH, we test the same model but assume cloud water pH is constant (pH = 4.5), which is according to an earlier study (Sofen et al., 2011), with

https://doi.org/10.5194/acp-2020-1279
Preprint. Discussion started: 12 January 2021


Atmospheric Chemistry and Physics Discussions

the purpose to examine the importance of changes in bulk cloud pH for modeled $\Delta^{17}O$. The $\Delta^{17}O(SO_4^{2-})$ values in the model were calculated by adding all sulfate isotope tracers with different $\Delta^{17}O$ end-members as described in Eqs. (1) to (4). The modeled $\Delta^{17}O(SO_4^{2-})$ values of grid including sampling sites were mass-weighted averaged within the troposphere.

2.4 Complementary data

2.4.1 Meteorological and black carbon data

The meteorological information was recorded by a Vantage Pro2 weather station (Davis Instruments) located at the QOMS. Measured meteorological parameters include temperature, RH, wind speed and air pressure with a precision of 0.1 °C, 1%, 0.1 m s^{-1} and 0.1 hPa, respectively. Precipitation data presented here was collected by manual measurements after each precipitation event. The airborne black carbon (BC) concentrations at the sampling site were measured by a newly developed Aethalometer model AE-33 (Magee Scientific), which was operated at an airflow rate of 4 L min^{-1} with a 1 min time resolution. By incorporating a patented DualSpot™ measurement method, the instrument can provide accurate real-time BC measurements. The detailed information on the BC observations is described in Chen et al. (2018).

2.4.2 O_3 mixing ratios

Since observations of O_3 at the sampling site are unavailable, the surface O_3 concentration in 2013 presented in this study are from an upwind region of our sampling site, i.e., NCO-P (Nepal Climate Observatory at Pyramid, 27.95°N, 86.80°E), which has been reported by Putero et al. (2018). This dataset was obtained from GAW/WDCRG (Global Atmosphere Watch programme/World Data Centre for Reactive Gases) hosted by EBAS data infrastructure at NILU (the Norwegian Institute for Air Research). Located in the southern slope of Mt. Everest, NCO-P is not far from our sampling site (~50 km), and the O_3 measurements there have been continuously performed with a UV-photometric analyzer (Thermo Scientific-Tei 49C) since year 2006 (Cristofanelli et al., 2010). In addition to O_3 concentration at NCO-P, the O_3 reanalysis data (at the level of 500 hPa) in 2018 for our sampling region (i.e. QOMS) was obtained from the ERA-Interim reanalysis (Dee et al., 2011) to further clarify the seasonality of O_3 over the southern TP.

2.4.3 Solar radiation and RH along with backward trajectories

Apart from the meteorological data directly observed at the sampling site, the solar radiation (SR) fluxes and RH along with backward trajectories arriving at the sampling sites during the sampling campaigns were also calculated by NOAA's HYSPLIT (Hybrid Single-Particle Lagrangian Integrated Trajectory) atmospheric transport and dispersion model, and averaged for each day (https://ready.arl.noaa.gov/HYSPLIT_traj.php) (Stein et al., 2015). The model calculation was forced by archived GDAS (Global Data Assimilation System) meteorological data obtained from NOAA Air Resource Laboratory with 1° × 1° latitude and longitude horizontal resolution. The calculated backward trajectories were clustered using TrajStat, an air mass trajectory statistical analysis tool contributed by Wang et al. (2009). Since the lifetime of sulfate aerosol is on the order of 4-5 d

https://doi.org/10.5194/acp-2020-1279
Preprint. Discussion started: 12 January 2021


Atmospheric Chemistry and Physics Discussions

(Alexander et al., 2012), the total run time of 120 h with time intervals of 3 h were adopted for each backward trajectory. Since the topography is characterized by huge relief differences in the Mt. Everest region, the arrival height of trajectories was set to 1000 m above the surface to reveal the long-range transport of air masses.

3 Results and discussion

3.1 Ionic characteristics and potential sulfate sources

Over the entire sampling campaign, concentrations of the main water-soluble ionic species (e.g., SO_4^{2-}, NO_3^-, Ca^{2+}, K^+) extracted from TSP samples in the Mt. Everest region show very similar and clear seasonal variations (Fig. 2a). That is, concentrations in the pre-monsoon seasons are 3-4 times higher than those during the monsoon season. It is likely the seasonal variations in the main ionic concentrations mainly result from the scavenging effect of precipitation in the monsoon season and more frequent dust storms in the pre-monsoon season (Kang et al., 2000). Our measurements indicate that SO_4^{2-} was the most abundant inorganic anion species followed by NO_3^-, while for cations, Ca^{2+} was the most abundant species. Although the Mt. Everest region is far from human activities, and is one of the most pristine areas in the world, we observed much higher sulfate concentrations ($[SO_4^{2-}]$) with an average of 9.4 ± 7.6 nmol m^{-3} during the sampling period in this region than those in the polar regions. For example, an annual mean $[SO_4^{2-}]$ of 1.7 nmol m^{-3} and 0.8 nmol m^{-3} was observed from Antarctic at the Dumont d'Urville station (DDU) and Dome C, respectively (Ishino et al., 2017; Hill-Falkenthal et al., 2013); Massling et al. (2015) reported seasonal mean values of $[SO_4^{2-}]$ within the range of 1.2 nmol m^{-3} to 5.0 nmol m^{-3} from the Northeast Greenland. The elevated $[SO_4^{2-}]$ in our study might suggest a significant contribution of long-range transported polluted air masses with sulfur sources.

Being located at high elevation and ~750 km away from the ocean, the Mt. Everest region is considered to possess a negligible amount of sea-salt sulfate in its air masses, which was also suggested by Cong et al. (2015a). In addition, the contribution of primary sulfate emitted from anthropogenic activity has been considered to be insignificant as compared to those from the secondary sulfate produced through oxidation of SO_2 (Berresheim et al., 1995). Thus, mineral dust is considered to be the only significant source of primary sulfate in our study due to frequently occurring dust storms (Fig. 3) as well as the significant correlations between SO_4^{2-} and Ca^{2+} in both seasons ($r = 0.825$, $p < 0.01$ for pre-monsoon; $r = 0.908$, $p < 0.01$ for monsoon) (Fig. 2b). Since Ca^{2+} is a typical tracer of crustal materials (dust) (Ram et al., 2010), here we use a mass ratio (k) of SO_4^{2-} to Ca^{2+} to correct sulfate concentrations and $\Delta^{17}O$ values for non-dust sulfate (nd-SO_4^{2-}) which can be regarded as secondary atmospheric sulfate (SAS). In addition, given that primary sulfate possesses 0‰ of $\Delta^{17}O$, $\Delta^{17}O$ values for nd-SO_4^{2-} ($\Delta^{17}O(SO_4^{2-})_{SAS}$) were calculated based on the following equations:

$$[\text{nd-}SO_4^{2-}] = [\text{bulk-}SO_4^{2-}] - k \times [Ca^{2+}] \quad (5)$$

https://doi.org/10.5194/acp-2020-1279
Preprint. Discussion started: 12 January 2021


Atmospheric Chemistry and Physics Discussions

$$\Delta^{17}O(SO_4^{2-})_{SAS} = [\text{bulk-}SO_4^{2-}] / [\text{nd-}SO_4^{2-}] \times \Delta^{17}O(SO_4^{2-})_{bulk} \quad (6)$$

where $[\text{bulk-}SO_4^{2-}]$ and $\Delta^{17}O(SO_4^{2-})_{bulk}$ represent concentration and $\Delta^{17}O$ value of bulk sulfate, respectively. Here we adopt a k value of 0.18, corresponding to a molar ratio of 0.075, which has been widely used in previous studies for the estimation of the terrigenous sulfate (Lin et al., 2020; Kunasek et al., 2010; Patris et al., 2002). Note that the k value of 0.59, corresponding to a molar ratio of 0.246, is known to be an upper limit as discussed in Kaufmann et al. (2010) and Goto-Azuma et al. (2019). If this upper limit of k value is adopted to the calculation this would result in higher $\Delta^{17}O(SO_4^{2-})_{SAS}$ values; however, the seasonal trend of $\Delta^{17}O(SO_4^{2-})_{SAS}$ as discussed below does not change and is even more pronounced (Fig. S1 in the Supplement). The uncertainties for $\Delta^{17}O(SO_4^{2-})_{SAS}$ values were estimated by propagating the uncertainties of $[SO_4^{2-}]$ and $[Ca^{2+}]$ (4%) as well as 1σ precision of corrected $\Delta^{17}O$ (0.1‰). All sulfate concentrations and the isotopic data are detailed in Table 1. The average contribution of terrigenous sulfate to the bulk sulfate is correspondingly calculated to be 6.3 ± 3.0%.

To identify the possible sources of air masses arriving at the Mt. Everest region during the sampling campaign, we analyzed the five-day backward trajectory of air masses (Fig. 1a). The results showed that the northward trajectories account for less than 10% of the total trajectories, and the air masses originated mainly from Nepal, northern/northeastern India, and Bangladesh. Previous studies have indicated that atmospheric brown clouds, basically layers of atmospheric pollution consisting of aerosols such as BC, dust, sulfate, and nitrate, extend from South Asia and accumulated on the southern slope of the Himalayas (Ramanathan et al., 2005; Kang et al., 2019; Wang et al., 2014). These South Asia-sourced pollutants can be transported into the TP region via the larger-scale atmospheric circulation and/or south-north-trending valley wind system (Cong et al., 2015a; Chen et al., 2018; Cong et al., 2015b; Xia et al., 2011). As a product of incomplete combustion of fossil fuel and biomass, BC deposited in the TP region has attracted much attention, since it can accelerate glacier melting, although the magnitude of this effect is uncertain (Kang et al., 2020 and references therein). Li et al. (2016) indicated that BC aerosols originating from Indo-Gangetic Plain can be transported to the Himalayas and even further to the southern TP. As shown in Fig. 2c, the $[\text{nd-}SO_4^{2-}]$ showed a consistent seasonality similar to [BC] during the sampling period, especially for the pre-monsoon season during which time a significant correlation ($r = 0.806$, $p < 0.01$) exists. Note that the insignificant correlation ($r = 0.434$, $p > 0.05$) in the monsoon season might be due to the much lower scavenging ratio of BC than that of SO_4^{2-} (Cerqueira et al., 2010). As a marker of biomass burning, $[K^+]$ also showed significant correlations with $[\text{nd-}SO_4^{2-}]$ in both seasons (r = 0.858, $p < 0.01$ for pre-monsoon; $r = 0.977$, $p < 0.01$ for monsoon) (Fig. 2d). Thus, it reasonable to suggest that combustion sources in South Asia contribute significantly to the atmospheric sulfate level in the Mt. Everest region, and even the entire southern TP.

3.2 $\Delta^{17}O$ signatures of sulfate and comparison with other sites

As listed in Table 1, the $\Delta^{17}O(SO_4^{2-})_{bulk}$ values in the Mt. Everest region range from 0.5‰ to 2.9‰ with an average of 1.5 ± 0.5‰ (weighted averaged at 1.3 ± 0.5‰), while for $\Delta^{17}O(SO_4^{2-})_{SAS}$, the values increased from 0.5‰ in the pre-monsoon to a

https://doi.org/10.5194/acp-2020-1279
Preprint. Discussion started: 12 January 2021


Atmospheric Chemistry and Physics Discussions

maximum of 3.0‰ in the monsoon season with an average of 1.7 ± 0.5‰ (weighted averaged at 1.4 ± 0.7‰). The difference in $\Delta^{17}O(SO_4^{2-})_{SAS}$ values between different seasons is statistically significant as suggested by a *t*-test ($p < 0.01$). In the pre-monsoon ($n = 13$), the $\Delta^{17}O(SO_4^{2-})_{SAS}$ values fell in the range from 0.5‰ to 1.7‰ with an average of 1.4 ± 0.5‰ (weighted averaged at 1.2 ± 0.6‰), which is obviously lower than that of 2.0 ± 0.5‰ (weighted averaged at 1.9 ± 0.7‰) in the monsoon season ($n = 11$) with a range from 1.3‰ to 3.0‰ (Fig. 4a). Additionally, no apparent correlation is observed between $\Delta^{17}O(SO_4^{2-})_{bulk}$ and [bulk-SO_4^{2-}] in any seasons indicating that the seasonality of $\Delta^{17}O(SO_4^{2-})_{bulk}$ was not controlled by the dust sourced sulfate with zero $\Delta^{17}O$ value.

While most measurements of $\Delta^{17}O(SO_4^{2-})$ conducted from mid-latitudes show weak seasonality in $\Delta^{17}O(SO_4^{2-})$ (e.g., Jenkins and Bao, 2006; Li et al., 2013; Lin et al., 2017), a clear seasonality was observed in the polar regions (Walters et al., 2019; Ishino et al., 2017; Hill-Falkenthal et al., 2013; McCabe et al., 2006). Figure 5 summarizes the available sulfate $\Delta^{17}O(SO_4^{2-})$ data so far in the present atmosphere (excluding ice core, gypcrete, volcanic ash, and soil) from different geographic areas, most of which stand for $\Delta^{17}O$ values in SAS. These observations indicate that atmospheric sulfate over much of the Earth's mid-latitude continents today appear to have relatively lower $\Delta^{17}O$ values (averaged at 1.0 ± 0.7‰, $n = 225$) than those observed from the polar regions (averaged at 1.6 ± 0.6‰, $n = 128$). We note that seasonality with minima in the summer and higher values in the autumn to spring was observed in polar regions (Walters et al., 2019; Ishino et al., 2017; Hill-Falkenthal et al., 2013; McCabe et al., 2006), as summarized in Fig. 5, which likely reflects a seasonal shift from OH- and H_2O_2- to O_3-dominated chemistry.

Our observed $\Delta^{17}O(SO_4^{2-})$ data in the Mt. Everest region (averaged at 1.7 ± 0.5‰) show higher values than those obtained from most of previous measurements at the similar latitude, and are comparable to those from the polar regions. Though the increase of $\Delta^{17}O(SO_4^{2-})_{SAS}$ values from pre-monsoon season (i.e. spring) to monsoon season (i.e. summer) is opposite to typical seasonality observed in polar regions (Fig. 5). Note that an average $\Delta^{17}O(SO_4^{2-})_{bulk}$ value of 1.1 ± 0.6‰ (n =4) was observed at the northern edge of the southern TP (Nam Co) within the pre-monsoon season (Lin et al., 2016). If SAS fractions for these Nam Co samples are corrected using the same method outlined previously, an average $\Delta^{17}O(SO_4^{2-})_{SAS}$ value of 2.1±1.1‰ is obtained (Lin et al., 2020). Several high $\Delta^{17}O(SO_4^{2-})_{SAS}$ values (averaged at 1.9 ± 0.3, $n = 6$) are also observed at a suburban site in the Sichuan Basin at Southwest China, likely due to inputs of sulfates transported from the Himalayas and Southern Tibetan Plateau via the westerly jet (Lin et al., 2020). These results are in agreement with our new measurements made at the Mt. Everest region, potentially indicating that the relatively higher $\Delta^{17}O(SO_4^{2-})_{SAS}$ might extensively exist within the southern TP and even its downwind region.

Due to the sunlight-driven seasonal changes in the photochemical activity, the oxidants with low or zero $\Delta^{17}O$ signature, e.g., HO_x, RO_x and H_2O_2, are more abundant in warm seasons relative to cold seasons. Accordingly, the $\Delta^{17}O$ values are expected to show a specific seasonal trend with minima in warm seasons and maxima in cold seasons. In fact, the seasonal trend of $\Delta^{17}O$

https://doi.org/10.5194/acp-2020-1279
Preprint. Discussion started: 12 January 2021

Atmospheric Chemistry and Physics Discussions

values in NO_3^- ($\Delta^{17}O(NO_3^-)$) in the same samples (Wang et al., 2020a) shows a typical seasonality (Fig. 4) reflecting the sunlight-driven seasonal changes in the photochemical oxidants, which has been reported in many previous studies conducted from diverse geographic sites (e.g., Michalski et al., 2003; Savarino et al., 2007; Guha et al., 2017; Wang et al., 2019b). Thus, the clear seasonal trend of high $\Delta^{17}O(SO_4^{2-})_{SAS}$ in warm season and low $\Delta^{17}O(SO_4^{2-})_{SAS}$ in cold season observed in the Mt. Everest region imply the existence of characteristic factor controlling sulfate formation.

3.3 Implications for the formation mechanism of sulfate in the Mt. Everest region

3.3.1 Contribution of stratospheric intrusion

Sulfate in the stratosphere, mainly produced by the reaction of SO_2 with OH (high $\Delta^{17}O$ in stratosphere due to lack of liquid water for isotopic exchange), has been suggested as a potential contributor to the relatively higher $\Delta^{17}O(SO_4^{2-})$ (Jenkins and Bao, 2006). Additionally, O_3 in stratosphere also has a higher $\Delta^{17}O$ value (34.2 ± 3.7‰ for bulk oxygen atoms) as compared with that in the troposphere (Krankowsky et al., 2000). Numerical simulations and field-based observations show that the Himalayas are a global hot spot for deep stratospheric intrusion (SI) in the springtime (pre-monsoon) (Škerlak et al., 2014; Lin et al., 2016; Lin et al., 2020). A recent study carried out at the southern TP and its downwind Southwest China observed high $\Delta^{17}O(SO_4^{2-})_{SAS}$ values in springtime aerosol samples that were influenced by the downward transport of stratospheric air, preliminary suggesting the potential causal link between $\Delta^{17}O(SO_4^{2-})_{SAS}$ values and the stratospheric influences (Lin et al., 2020). We therefore first evaluate the potential stratospheric influence on the relatively higher $\Delta^{17}O(SO_4^{2-})_{SAS}$ values in our study. Previous studies suggest that SI frequency at the southern TP is generally lower in summer than spring (Priyadarshi et al., 2014; Zheng et al., 2011; Yin et al., 2017). $\Delta^{17}O(SO_4^{2-})_{SAS}$ in our study, however, displays higher values in summer than spring. Consequently, the observed high $\Delta^{17}O(SO_4^{2-})_{SAS}$ values, especially in summer, may not be predominately explained by the stratospheric influences. The stratospheric contribution to each individual sample, which may be quantified and constrained in the future by simultaneous measurements of chemical tracers for stratospheric air masses, is beyond the scope of this study. In the ensuing sections, we focus on the role of sulfate formation mechanisms in the troposphere in elevating $\Delta^{17}O(SO_4^{2-})_{SAS}$ values.

3.3.2 Importance of S(IV) + O_3 oxidation pathways

Given that the $\Delta^{17}O(SO_4^{2-})$ signatures for the sulfate formation pathways are all lower than 0.8‰ except for the S(IV) + O_3 pathway ($\Delta^{17}O(SO_4^{2-})$ = 6.5 ± 0.3‰), the atmospheric sulfate with $\Delta^{17}O(SO_4^{2-})_{SAS}$ > 1‰ clearly indicate role of O_3 in sulfate production. The high $\Delta^{17}O(SO_4^{2-})_{SAS}$ values with an average of 1.7 ± 0.5‰ in the Mt. Everest region suggest a significant role of oxidation of S(IV) by O_3 in the formation of atmospheric sulfate in this region. Here, by applying a simple isotope mass-balance method (Eqs. (7) and (8)) (Walters et al., 2019), we calculated the maximum contribution of oxidation by O_3 ($f_{O3,\,max}$)

https://doi.org/10.5194/acp-2020-1279
Preprint. Discussion started: 12 January 2021

Atmospheric Chemistry and Physics Discussions

to SAS production by assuming no contribution from oxidation by H_2O_2, and the minimum contribution ($f_{O3,\,min}$) was estimated by assuming that H_2O_2 is the only other oxidant.

$$f_{O3,\,max} = \Delta^{17}O(SO_4^{2-})_{SAS} / \Delta^{17}O(SO_4^{2-})_{O3} \quad (7)$$

$$f_{O3,\,min} = (\Delta^{17}O(SO_4^{2-})_{SAS} - \Delta^{17}O(SO_4^{2-})_{H2O2}) / (\Delta^{17}O(SO_4^{2-})_{O3} - \Delta^{17}O(SO_4^{2-})_{H2O2}) \quad (8)$$

where $\Delta^{17}O(SO_4^{2-})_{O3}$ = 6.5 ± 0.3‰, and $\Delta^{17}O(SO_4^{2-})_{H2O2}$ = 0.8 ± 0.2‰ as indicated above. The results show an estimated O_3 contribution range ($f_{O3,\,min}$ to $f_{O3,\,max}$) of 15 ± 10% to 25 ± 9% corresponding to the mean $\Delta^{17}O(SO_4^{2-})_{SAS}$ value of 1.7 ± 0.5‰ for the entire sampling period. Based on the seasonal average $\Delta^{17}O(SO_4^{2-})_{SAS}$ values (1.4 ± 0.5‰ for pre-monsoon and 2.0 ± 0.5‰ for monsoon) and estimation of f_{O3} by the above isotope mass-balance method, the f_{O3} fell in a range of 10 ± 9% to 21 ± 8% and 21 ± 9% to 31 ± 8% for the pre-monsoon and monsoon seasons, respectively. The relative contribution of aqueous oxidation by O_3 is significantly higher in the monsoon than in the pre-monsoon season.

In Fig. 6, we compare the seasonal variation of observed $\Delta^{17}O(SO_4^{2-})_{SAS}$ with these meteorological parameters in this region. Interestingly, the RH at QOMS during the sampling period shows co-variation with our observed $\Delta^{17}O(SO_4^{2-})_{SAS}$ with a statistically significant correlation (r = 0.845, p < 0.05), although this correlation between $\Delta^{17}O(SO_4^{2-})_{SAS}$ and RH along with the air-mass transport pathways shows less significantly (r = 0.697, p = 0.124) (Figs. 6a and 6b). In contrast, tropospheric O_3 concentrations, acquired from the both northern and southern slopes of Mt. Everest at the QOMS and NCO-P, show seasonal variations with significantly higher levels in the pre-monsoon season than in the monsoon season (Figs. 6c and 6d), indicating that O_3 abundance is not the ultimate determinant of seasonal variation in $\Delta^{17}O(SO_4^{2-})_{SAS}$. The SR along with the air-mass transport pathways was stronger in the pre-monsoon season than in the monsoon season, which might hypothesize the seasonality of $\Delta^{17}O(SO_4^{2-})_{SAS}$ via facilitating SO_2 oxidation by OH ($\Delta^{17}O(SO_4^{2-})$ = 0‰). However, if this is the case, relatively lower $\Delta^{17}O(NO_3^-)$ values should be observed in the pre-monsoon season due to enhancement of NO_2 + OH pathways producing low $\Delta^{17}O(NO_3^-)$values, but this variation were not observed (Fig. 4b & Wang et al., 2020a). Thus, this hypothesis is not likely to dominate the characteristic $\Delta^{17}O(SO_4^{2-})_{SAS}$ values in the Mt. Everest region. Although we cannot extract clear relations of $\Delta^{17}O(SO_4^{2-})_{SAS}$ with the meteorological parameters, the relatively high $\Delta^{17}O(SO_4^{2-})_{SAS}$ in this region imply the importance of aqueous oxidation of S(IV) by O_3. We therefore discuss the importance of atmospheric acidity in the aqueous phase chemistry as factor controlling the S(IV) + O_3 oxidation pathway in the next section.

3.3.3 Importance of atmospheric acidity for sulfate formation pathways

The aqueous oxidation of S(IV) by O_3 is only significant at high pH conditions greater than pH = 5, due to the strong pH dependence of S(IV) species in solutions (Calvert et al., 1985; Seinfeld and Pandis, 2016). At the pH below 5, H_2O_2 is considered to dominate aqueous sulfate production. Since the pH in modern cloud water is typically within the range of 3 to 5 (Pye et al., 2020 and references therein), the aqueous oxidation of S(IV) by O_3 is thus considered to be unimportant when

https://doi.org/10.5194/acp-2020-1279
Preprint. Discussion started: 12 January 2021

Atmospheric Chemistry and Physics Discussions

compared to the oxidation by H_2O_2. However, our observed high $\Delta^{17}O(SO_4^{2-})_{SAS}$ values suggest the importance of sulfate formation by aqueous oxidation of S(IV) by O_3, indicating that sulfate formation is occurring at relatively high pH conditions. Indeed, the pH in fog, rain and snow in the TP region were reported to be high, respectively, pH = 6.4, 6.2, and 5.96 ± 0.54 (Wang et al., 2019a; Kang et al., 2002), and the modeled cloud water pH in the Mt. Everest region and the South Asia showed approximately pH = 6 (Shah et al., 2020; Pye et al., 2020). Such high pH condition favors S(IV) oxidation by O_3. We suggest that the frequently occurring dust storms, not only in the Mt. Everest region but also in South Asia (Fig. 3 & Prospero et al., 2002), are likely to play an important role for promoting the S(IV) oxidation by O_3 through the high cloud water pH conditions. Consequently, our findings provide an important observational basis for better constraints on the importance of pH in sulfate formation pathways.

To examine the importance of cloud water pH and sulfate formation on dust surface, we conducted model simulations by GEOS-Chem in three cases including (i) fixed cloud water pH (= 4.5) and no consideration of sulfate formation on dust surface, (ii) variable cloud water pH and no consideration of sulfate formation on dust surface, and (iii) variable cloud water pH and consideration of sulfate formation on dust surface. The results show that, if the cloud water pH is fixed to 4.5, the modeled monthly-mean $\Delta^{17}O(SO_4^{2-})_{SAS}$ values range from 0.5‰ to 0.7‰ during the sampling period (April to September), significantly lower than the observed monthly weighted average $\Delta^{17}O(SO_4^{2-})_{SAS}$ values with a range of 1.0‰ to 2.1‰ in the Mt. Everest region (Fig. 7a). On the other hand, when considering variable cloud water pH (i.e. cases (ii) and (iii)), the modeled $\Delta^{17}O(SO_4^{2-})_{SAS}$ values increase markedly with a range of 1.1‰ to 2.2‰ (Fig. 7a). The increases of modeled $\Delta^{17}O(SO_4^{2-})_{SAS}$ when calculating cloud water pH are due to increases of the modeled f_{O3} from 5 ± 1% in case (i) to 24 ± 6% in cases (ii) and/or (iii). In addition to the magnitude of $\Delta^{17}O(SO_4^{2-})$, f_{O3} are also well reproduced by the model simulations in cases (ii) and (iii). During the sampling period, the modeled monthly-mean f_{O3} in cases (ii) and (iii) varied from 14% to 31% with an average of 24 ± 6%, which shows a good agreement with f_{O3} calculated based on Eqs. (7) and (8) (15 ± 10% for $f_{O3,\,min}$ and 25 ± 9% for $f_{O3,\,max}$, respectively). It is important to note that the modeled f_{O3} in cases (ii) and/or (iii) is even higher than the modeled f_{H2O2} (averaged at 20 ± 7%). Also, as shown in Fig. 7d, the modeled heterogeneous S(IV) oxidation on dust surface also play a role for producing high $\Delta^{17}O(SO_4^{2-})$ values, particularly in the pre-monsoon season, but the modeled relative contribution of this pathway does not exceed 5% to the total sulfate production.

Our result with high $\Delta^{17}O(SO_4^{2-})_{SAS}$ found in the Mt. Everest region, in turn, highlights observational evidence that atmospheric acidity plays an important role in controlling sulfate formation pathways particularly for dust-rich environments. For typical earlier studies until the 1990s, pH of cloud droplet was considered too low to promote the S(IV) + O_3 reaction for sulfate formation (Chin et al., 1996; Koch et al., 1999). Although recent studies have proposed the importance of the cloud water pH promoting the S(IV) + O_3 pathway to estimate atmospheric sulfate formation (Paulot et al., 2014; Banzhaf et al., 2012), even the latest study (Turnock et al., 2019) still prescribes a constant cloud pH in the estimation for radiative forcing effect via aerosols. Consequently, accurate estimate of cloud water pH in the model simulation and elucidation of its relation to

https://doi.org/10.5194/acp-2020-1279
Preprint. Discussion started: 12 January 2021


Atmospheric Chemistry and Physics Discussions

405 atmospheric sulfate formation are necessary for precise model forecasts, and observations of $\Delta^{17}O(SO_4^{2-})_{SAS}$ are important constraints on model validation.

3.3.4 Possible importance of atmospheric humidity on $\Delta^{17}O(SO_4^{2-})$

Although the model in this study predicted minor relative contribution of heterogeneous oxidation of SO_2 by O_3 on dust surface (Fig. 7d), it is worth noting the possible importance of this pathway. In a laboratory study, Ullerstam et al. (2002) observed a 410 47% increase in the amount of sulfate formed via SO_2 oxidation by O_3 on dust surface when dust samples were exposed to a RH of 80% as compared to an experiment without the intermittent water exposure. Taken together with the co-variation between $\Delta^{17}O(SO_4^{2-})_{SAS}$ and RH as described above (Figs. 7a and 7b), there is a possibility that the ubiquitous alkaline dust aerosol extending from South Asia to the Mt. Everest region as reported in previous studies (e.g., Wang et al., 2020b; Prospero et al., 2002) render a suitable condition for S(IV) oxidation by O_3 especially during the monsoon season. Given that soluble 415 Ca^{2+} and Mg^{2+}, those being thought to provide alkalinity, mostly exist as coarse-mode particles larger than 1 μm (Yang et al., 2016), size distributions of sulfate concentration and $\Delta^{17}O(SO_4^{2-})_{SAS}$ for dust-rich environments would provide a detailed consequence for the importance of heterogeneous oxidation of SO_2 by O_3 on the dust surface in the future study.

4 Conclusions

In this study, we report observations of sulfate concentrations and $\Delta^{17}O(SO_4^{2-})$ in aerosols samples collected from the Mt. 420 Everest region over a period including pre-monsoon and monsoon seasons in 2018. The combustion tracers (i.e., BC and K^+) as well as the backward trajectories of air masses suggest a combustion of sources (e.g., fossil fuel and biomass combustion) in South Asia contributed significantly to the observed sulfate. The average $\Delta^{17}O(SO_4^{2-})_{SAS}$ value of 1.7 ± 0.5‰ observed from the Mt. Everest region is higher than the published data reported from the Earth's mid-latitude continents which have relatively lower $\Delta^{17}O(SO_4^{2-})$ values (1.0 ± 0.7‰). Intriguingly, a seasonal variation of $\Delta^{17}O(SO_4^{2-})_{SAS}$ with high values in monsoon (warm 425 season) and low values in pre-monsoon (cold season) was observed in this study, which is opposite to that of $\Delta^{17}O(NO_3^-)$ measured from the same aerosol samples as well as that of $\Delta^{17}O(SO_4^{2-})_{SAS}$ observed from the polar regions. The relatively high $\Delta^{17}O(SO_4^{2-})_{SAS}$ in this region imply the importance of aqueous oxidation of S(IV) by O_3 which is favored by high pH conditions. An updated global three-dimensional chemical transport model with high pH condition better reproduced the observed high $\Delta^{17}O(SO_4^{2-})_{SAS}$ values in the Mt. Everest region. As illustrated in Fig. 8, we propose that the S(IV) oxidation by O_3 during long-430 range transport over the Himalayas contributes significantly to sulfate levels in the Mt. Everest region, and even the entire southern TP. Overall, our study provides observational evidence that atmospheric acidity plays an important role in controlling sulfate formation pathways particularly for dust-rich environments. Such identification of key processes provides an important

https://doi.org/10.5194/acp-2020-1279
Preprint. Discussion started: 12 January 2021

basis for better understanding of the sulfur cycle in the TP, which is further meaningful to accurately evaluate the environment and climatic changes within this region.

Data availability. The data used for the figures and the interpretations have been included in the Supplement.

Author contributions. KW, SK, and SH designed the study. KW and SK organized the Mt. Everest field campaign, and collected samples. SH, KW, ML, SI, and KK carried out the experiments. SH, SI, and BA performed the model simulations and analysis. KW and SH analyzed the data with contributions from SK, ML, BA and NY. KW and SH prepare the manuscript with contributions from all other co-authors.

Competing interests. The authors declare that they have no conflict of interest.

Acknowledgements. This project was financially supported by the second Tibetan Plateau Scientific Expedition and Research Program (STEP) (No. 2019QZKK0605), and the National Natural Science Foundation of China (Nos. 41705132 [S.K.], 41630754 [S.K.], 42021002 [M.L.]). K.W. acknowledges the China Scholarship Council under No. 201804910810. This work was carried out within a framework across the Tibetan Plateau: Atmospheric Pollution and Cryospheric Change (APCC). We would like to thank the staff working at the Qomolangma Station for Atmospheric and Environmental Observation and Research, Chinese Academy of Sciences for their valuable help with field sampling and supplying the meteorological dataset. Also, We acknowledge CNR-ISAC (Institute of Atmospheric Sciences and Climate of the National Research Council of Italy) and Ev-K2-CNR Chartered Association for providing O_3 dataset at NCO-P and managing/supporting the NCO-P station as well as the on-site scientific operation. The authors also thank European Centre for Medium-range Weather Forecast for the ERA-Interim reanalysis dataset (https://www.ecmwf.int/en/forecasts/datasets/reanalysis-datasets/era-interim). The authors gratefully acknowledge the NOAA Air Resources Laboratory for the provision of the HYSPLIT transport and dispersion model and/or READY website (https://www.ready.noaa.gov) used in this publication. This study was also supported by Japan Society for the Promotion of Science (JSPS) KAKENHI (Grants JP18F18113 [N.Y.], JP18K19850 [S.H.], JP19H01143 [S.H.], JP20H04305 [S.H.], JP16H05884 [S.H.], and JP17H06105 [N.Y.]) from the Ministry of Education, Culture, Sports, Science and Technology (MEXT), Japan. B.A. acknowledges support from NSF AGS 1644998.

References

Alexander, B., Savarino, J., Barkov, N., Delmas, R., and Thiemens, M.: Climate driven changes in the oxidation pathways of atmospheric sulfur, Geophys. Res. Lett., 29, 1685, https://doi.org/10.1029/2002GL014879, 2002.

Alexander, B., Park, R. J., Jacob, D. J., Li, Q., Yantosca, R. M., Savarino, J., Lee, C., and Thiemens, M.: Sulfate formation in sea-salt aerosols: Constraints from oxygen isotopes, J. Geophys. Res. Atmos., 110, https://doi.org/10.1029/2004JD005659, 2005.

Alexander, B., Park, R. J., Jacob, D. J., and Gong, S.: Transition metal-catalyzed oxidation of atmospheric sulfur: Global implications for the sulfur budget, J. Geophys. Res., 114, https://doi.org/10.1029/2008JD010486, 2009.

https://doi.org/10.5194/acp-2020-1279
Preprint. Discussion started: 12 January 2021

Alexander, B., Allman, D., Amos, H., Fairlie, T., Dachs, J., Hegg, D. A., and Sletten, R. S.: Isotopic constraints on the formation pathways of sulfate aerosol in the marine boundary layer of the subtropical northeast Atlantic Ocean, J. Geophys. Res. Atmos., 117, https://doi.org/10.1029/2011JD016773, 2012.

Banzhaf, S., Schaap, M., Kerschbaumer, A., Reimer, E., Stern, R., Van Der Swaluw, E., and Builtjes, P.: Implementation and evaluation of pH-dependent cloud chemistry and wet deposition in the chemical transport model REM-Calgrid, Atmos. Environ., 49, 378-390, https://doi.org/10.1016/j.atmosenv.2011.10.069, 2012.

Bao, H., Michalski, G. M., and Thiemens, M. H.: Sulfate oxygen-17 anomalies in desert varnishes, Geochim. Cosmochim. Acta, 65, 2029-2036, https://doi.org/10.1016/S0016-7037(00)00490-7, 2001.

Bao, H., and Reheis, M. C.: Multiple oxygen and sulfur isotopic analyses on water-soluble sulfate in bulk atmospheric deposition from the southwestern United States, J. Geophys. Res. Atmos., 108, https://doi.org/10.1029/2002JD003022, 2003.

Berresheim, H., Wine, P., and Davis, D.: Sulfur in the atmosphere, in: Composition, chemistry, and climate of the atmosphere, edited by: Singh, H. B., Van Nostrand Reinhold, New York, 251-307, 1995.

Bey, I., Jacob, D. J., Yantosca, R. M., Logan, J. A., Field, B. D., Fiore, A. M., Li, Q., Liu, H. Y., Mickley, L. J., and Schultz, M. G.: Global modeling of tropospheric chemistry with assimilated meteorology: Model description and evaluation, J. Geophys. Res. Atmos., 106, 23073-23095, https://doi.org/10.1029/2001jd000807, 2001.

Calvert, J. G., Lazrus, A., Kok, G. L., Heikes, B. G., Walega, J. G., Lind, J., and Cantrell, C. A.: Chemical mechanisms of acid generation in the troposphere, Nature, 317, 27-35, https://doi.org/10.1038/317027a0, 1985.

Cerqueira, M., Pio, C., Legrand, M., Puxbaum, H., Kasper-Giebl, A., Afonso, J., Preunkert, S., Gelencsér, A., and Fialho, P.: Particulate carbon in precipitation at European background sites, J. Aerosol Sci., 41, 51-61, https://doi.org/10.1016/j.jaerosci.2009.08.002, 2010.

Chang, J., Brost, R., Isaksen, I., Madronich, S., Middleton, P., Stockwell, W., and Walcek, C.: A three-dimensional Eulerian acid deposition model: Physical concepts and formulation, J. Geophys. Res. Atmos., 92, 14681-14700, https://doi.org/10.1029/jd092id12p14681, 1987.

Charlson, R. J., Schwartz, S., Hales, J., Cess, R. D., Coakley, J. J., Hansen, J., and Hofmann, D.: Climate forcing by anthropogenic aerosols, Science, 255, 423-430, https://doi.org/10.1126/science.255.5043.423, 1992.

Chen, Q., Geng, L., Schmidt, J. A., Xie, Z., Kang, H., Dachs, J., Cole-Dai, J., Schauer, A. J., Camp, M. G., and Alexander, B.: Isotopic constraints on the role of hypohalous acids in sulfate aerosol formation in the remote marine boundary layer, Atmos. Chem. Phys., 16, 11433-11450, https://doi.org/10.5194/acp-16-11433-2016, 2016.

Chen, Q., Schmidt, J. A., Shah, V., Jaeglé, L., Sherwen, T., and Alexander, B.: Sulfate production by reactive bromine: Implications for the global sulfur and reactive bromine budgets, Geophys. Res. Lett., 44, 7069-7078, https://doi.org/10.1002/2017gl073812, 2017.

Chen, X., Kang, S., Cong, Z., Yang, J., and Ma, Y.: Concentration, temporal variation, and sources of black carbon in the Mt. Everest region retrieved by real-time observation and simulation, Atmos. Chem. Phys., 18, 12859-12875, https://doi.org/10.5194/acp-18-12859-2018, 2018.

Chin, M., Jacob, D. J., Gardner, G. M., Foreman-Fowler, M. S., Spiro, P. A., and Savoie, D. L.: A global three-dimensional model of tropospheric sulfate, J. Geophys. Res. Atmos., 101, 18667-18690, https://doi.org/10.1029/96jd01221, 1996.

Cong, Z., Kang, S., Kawamura, K., Liu, B., Wan, X., Wang, Z., Gao, S., and Fu, P.: Carbonaceous aerosols on the south edge of the Tibetan Plateau: concentrations, seasonality and sources, Atmos. Chem. Phys., 15, 1573-1584, https://doi.org/10.5194/acp-15-1573-2015, 2015a.

Cong, Z., Kawamura, K., Kang, S., and Fu, P.: Penetration of biomass-burning emissions from South Asia through the Himalayas: new insights from atmospheric organic acids, Sci. Rep., 5, 9580, https://doi.org/10.1038/srep09580, 2015b.

Cristofanelli, P., Bracci, A., Sprenger, M., Marinoni, A., Bonafe, U., Calzolari, F., Duchi, R., Laj, P., Roccato, F., and Venzac, H.: Tropospheric ozone variations at the Nepal climate observatory-pyramid (Himalayas, 5079m a.s.l.) and influence of stratospheric intrusion events, Atmos. Chem. Phys., 10, 6537-6549, https://doi.org/10.5194/acp-10-6537-2010, 2010.

Dee, D. P., Uppala, S. M., Simmons, A., Berrisford, P., Poli, P., Kobayashi, S., Andrae, U., Balmaseda, M., Balsamo, G., and Bauer, d. P.: The ERA-Interim reanalysis: Configuration and performance of the data assimilation system, Q. J. R. Meteorolog. Soc., 137, 553-597, https://doi.org/10.1002/qj.828, 2011.

Dentener, F., Williams, J., and Metzger, S.: Aqueous phase reaction of HNO_4: The impact on tropospheric chemistry, J. Atmos. Chem., 41, 109-133, https://doi.org/10.1023/A:1014233910126, 2002.

https://doi.org/10.5194/acp-2020-1279
Preprint. Discussion started: 12 January 2021

Dominguez, G., Jackson, T., Brothers, L., Barnett, B., Nguyen, B., and Thiemens, M. H.: Discovery and measurement of an isotopically distinct source of sulfate in Earth's atmosphere, Proc. Natl. Acad. Sci. U.S.A., 105, 12769-12773, https://doi.org/10.1073/pnas.0805255105, 2008.

Duan, J., Esper, J., Buntgen, U., Li, L., Xoplaki, E., Zhang, H., Wang, L., Fang, Y., and Luterbacher, J.: Weakening of annual temperature cycle over the Tibetan Plateau since the 1870s, Nat. Commun., 8, 14008-14008, https://doi.org/10.1038/ncomms14008, 2017.

Fairlie, T. D., Jacob, D. J., and Park, R. J.: The impact of transpacific transport of mineral dust in the United States, Atmos. Environ., 41, 1251-1266, https://doi.org/10.1016/j.atmosenv.2006.09.048, 2007.

Fairlie, T. D., Jacob, D. J., Dibb, J. E., Alexander, B., Avery, M. A., van Donkelaar, A., and Zhang, L.: Impact of mineral dust on nitrate, sulfate, and ozone in transpacific Asian pollution plumes, Atmos. Chem. Phys., 10, 3999-4012, https://doi.org/10.5194/acp-10-3999-2010, 2010.

Feingold, G., Frost, G. J., and Ravishankara, A.: Role of NO_3 in sulfate production in the wintertime northern latitudes, J. Geophys. Res. Atmos., 107, 4640, https://doi.org/10.1029/2002jd002288, 2002.

Gautier, E., Savarino, J., Hoek, J., Erbland, J., Caillon, N., Hattori, S., Yoshida, N., Albalat, E., Albarede, F., and Farquhar, J.: 2600-years of stratospheric volcanism through sulfate isotopes, Nat. Commun., 10, 1-7, https://doi.org/10.1038/s41467-019-08357-0, 2019.

Geng, L., Schauer, A. J., Kunasek, S. A., Sofen, E. D., Erbland, J., Savarino, J., Allman, D. J., Sletten, R. S., and Alexander, B.: Analysis of oxygen-17 excess of nitrate and sulfate at sub-micromole levels using the pyrolysis method, Rapid Commun. Mass Spectrom., 27, 2411-2419, https://doi.org/10.1002/rcm.6703, 2013.

Goto-Azuma, K., Hirabayashi, M., Motoyama, H., Miyake, T., Kuramoto, T., Uemura, R., Igarashi, M., Iizuka, Y., Sakurai, T., and Horikawa, S.: Reduced marine phytoplankton sulphur emissions in the Southern Ocean during the past seven glacials, Nat. Commun., 10, 1-7, https://doi.org/10.1038/s41467-019-11128-6, 2019.

Guha, T., Lin, C., Bhattacharya, S., Mahajan, A., Ou Yang, C., Lan, Y., Hsu, S., and Liang, M.: Isotopic ratios of nitrate in aerosol samples from Mt. Lulin, a high-altitude station in Central Taiwan, Atmos. Environ., 154, 53-69, https://doi.org/10.1016/j.atmosenv.2017.01.036, 2017.

Harris, E., Sinha, B., Van Pinxteren, D., Tilgner, A., Fomba, K. W., Schneider, J., Roth, A., Gnauk, T., Fahlbusch, B., and Mertes, S.: Enhanced role of transition metal ion catalysis during in-cloud oxidation of SO_2, Science, 340, 727-730, https://doi.org/10.1126/science.1230911, 2013.

He, P., Alexander, B., Geng, L., Chi, X., Fan, S., Zhan, H., Kang, H., Zheng, G., Cheng, Y., and Su, H.: Isotopic constraints on heterogeneous sulfate production in Beijing haze, Atmos. Chem. Phys., 18, 5515-5528, https://doi.org/10.5194/acp-18-5515-2018, 2018.

Hill-Falkenthal, J., Priyadarshi, A., Savarino, J., and Thiemens, M.: Seasonal variations in ^{35}S and $\Delta^{17}O$ of sulfate aerosols on the Antarctic plateau, J. Geophys. Res. Atmos., 118, 9444-9455, https://doi.org/10.1002/jgrd.50716, 2013.

Hoesly, R. M., Smith, S. J., Feng, L., Klimont, Z., Janssens-Maenhout, G., Pitkanen, T., Seibert, J. J., Vu, L., Andres, R. J., and Bolt, R. M.: Historical (1750-2014) anthropogenic emissions of reactive gases and aerosols from the Community Emission Data System (CEDS), Geosci. Model Dev., 11, 369-408, https://doi.org/10.5194/gmd-11-369-2018, 2018.

Holt, B., Kumar, R., and Cunningham, P.: Oxygen-18 study of the aqueous-phase oxidation of sulfur dioxide, Atmos. Environ., 15, 557-566, https://doi.org/10.1016/0004-6981(81)90186-4, 1981.

Immerzeel, W. W., Van Beek, L. P., and Bierkens, M. F.: Climate change will affect the Asian water towers, Science, 328, 1382-1385, https://doi.org/10.1126/science.1183188, 2010.

Ishino, S., Hattori, S., Savarino, J., Jourdain, B., Preunkert, S., Legrand, M., Caillon, N., Barbero, A., Kuribayashi, K., and Yoshida, N.: Seasonal variations of triple oxygen isotopic compositions of atmospheric sulfate, nitrate, and ozone at Dumont d'Urville, coastal Antarctica, Atmos. Chem. Phys., 17, 3713-3727, https://doi.org/10.5194/acp-17-3713-2017, 2017.

Ishino, S., and Hattori, S.: Datasets for "Regional characteristics of atmospheric sulfate formation in East Antarctica imprinted on 17O-excess signature", Mendeley Data, V1, doi: 10.17632/xfr8ffn9xv.1, 2020.

Jenkins, K. A., and Bao, H.: Multiple oxygen and sulfur isotope compositions of atmospheric sulfate in Baton Rouge, LA, USA, Atmos. Environ., 40, 4528-4537, https://doi.org/10.1016/j.atmosenv.2006.04.010, 2006.

Kang, S., Wake, C. P., Qin, D., Mayewski, P. A., and Yao, T.: Monsoon and dust signals recorded in Dasuopu glacier, Tibetan Plateau, J. Glaciol., 46, 222-226, https://doi.org/10.3189/172756500781832864, 2000.

https://doi.org/10.5194/acp-2020-1279
Preprint. Discussion started: 12 January 2021

Atmospheric Chemistry and Physics Discussions

Kang, S., Qin, D., Mayewski, P. A., Sneed, S. B., and Yao, T.: Chemical composition of fresh snow on Xixabangma peak, central Himalaya, during the summer monsoon season, J. Glaciol., 48, 337-339, https://doi.org/10.3189/172756502781831467, 2002.

Kang, S., You, Q., Flügel, W. A., Pepin, N., and Yao, T.: Review of climate and cryospheric change in the Tibetan Plateau, Environ. Res. Lett., 5, 015101, https://doi.org/10.1088/1748-9326/5/1/015101, 2010.

Kang, S., Zhang, Q., Qian, Y., Ji, Z., Li, C., Cong, Z., Zhang, Y., Guo, J., Du, W., and Huang, J.: Linking Atmospheric Pollution to Cryospheric Change in the Third Pole Region: Current Progresses and Future Prospects, Natl. Sci. Rev., 6, 796-809, https://doi.org/10.1093/nsr/nwz031, 2019.

Kang, S., Zhang, Y., Qian, Y., and Wang, H.: A review of black carbon in snow and ice and its impact on the cryosphere, Earth Sci. Rev., 103346, https://doi.org/10.1016/j.earscirev.2020.103346, 2020.

Kaufman, Y. J., and Tanre, D.: Effect of variations in super-saturation on the formation of cloud condensation nuclei, Nature, 369, 45-48, https://doi.org/10.1038/369045a0, 1994.

Kaufmann, P., Fundel, F., Fischer, H., Bigler, M., Ruth, U., Udisti, R., Hansson, M., De Angelis, M., Barbante, C., and Wolff, E. W.: Ammonium and non-sea salt sulfate in the EPICA ice cores as indicator of biological activity in the Southern Ocean, Quat. Sci. Rev., 29, 313-323, https://doi.org/10.1016/j.quascirev.2009.11.009, 2010.

Koch, D., Jacob, D., Tegen, I., Rind, D., and Chin, M.: Tropospheric sulfur simulation and sulfate direct radiative forcing in the Goddard Institute for Space Studies general circulation model, J. Geophys. Res. Atmos., 104, 23799-23822, https://doi.org/10.1029/1999jd900248, 1999.

Krankowsky, D., Lämmerzahl, P., and Mauersberger, K.: Isotopic measurements of stratospheric ozone, Geophys. Res. Lett., 27, 2593-2595, https://doi.org/10.1029/2000gl011812, 2000.

Kulmala, M., Pirjola, L., and Mäkelä, J. M.: Stable sulphate clusters as a source of new atmospheric particles, Nature, 404, 66-69, https://doi.org/10.1038/35003550, 2000.

Kunasek, S., Alexander, B., Steig, E., Sofen, E., Jackson, T., Thiemens, M., McConnell, J., Gleason, D., and Amos, H.: Sulfate sources and oxidation chemistry over the past 230 years from sulfur and oxygen isotopes of sulfate in a West Antarctic ice core, J. Geophys. Res. Atmos., 115, https://doi.org/10.1029/2010jd013846, 2010.

Lee, C. W., and Thiemens, M. H.: The $\delta^{17}O$ and $\delta^{18}O$ measurements of atmospheric sulfate from a coastal and high alpine region: A mass-independent isotopic anomaly, J. Geophys. Res. Atmos., 106, 17359-17374, https://doi.org/10.1029/2000jd900805, 2001.

Lee, Y., and Schwartz, S. E.: Kinetics of oxidation of aqueous sulfur (IV) by nitrogen dioxide, in: Precipitation Scavenging, Dry Deposition and Resuspension, edited by: Pruppacher, H. R., Semonin, R. G., and Slinn, W. G. N., Elsevier, New York, 453-470, 1983.

Li, C., Bosch, C., Kang, S., Andersson, A., Chen, P., Zhang, Q., Cong, Z., Chen, B., Qin, D., and Gustafsson, Ö.: Sources of black carbon to the Himalayan-Tibetan Plateau glaciers, Nat. Commun., 7, 1-7, https://doi.org/10.1038/ncomms12574, 2016.

Li, X., Bao, H., Gan, Y., Zhou, A., and Liu, Y.: Multiple oxygen and sulfur isotope compositions of secondary atmospheric sulfate in a mega-city in central China, Atmos. Environ., 81, 591-599, https://doi.org/10.1016/j.atmosenv.2013.09.051, 2013.

Liang, J., and Jacobson, M. Z.: A study of sulfur dioxide oxidation pathways over a range of liquid water contents, pH values, and temperatures, J. Geophys. Res. Atmos., 104, 13749-13769, https://doi.org/10.1029/1999jd900097, 1999.

Lin, M., Zhang, Z., Su, L., Hill-Falkenthal, J., Priyadarshi, A., Zhang, Q., Zhang, G., Kang, S., Chan, C. Y., and Thiemens, M. H.: Resolving the impact of stratosphere-to-troposphere transport on the sulfur cycle and surface ozone over the Tibetan Plateau using a cosmogenic ^{35}S tracer, J. Geophys. Res. Atmos., 121, 439-456, https://doi.org/10.1002/2015jd023801, 2016.

Lin, M., Biglari, S., Zhang, Z., Crocker, D., Tao, J., Su, B., Liu, L., and Thiemens, M. H.: Vertically uniform formation pathways of tropospheric sulfate aerosols in East China detected from triple stable oxygen and radiogenic sulfur isotopes, Geophys. Res. Lett., 44, 5187-5196, https://doi.org/10.1002/2017gl073637, 2017.

Lin, M., Wang, K., Kang, S., Li, Y., Fan, Z., and Thiemens, M. H.: Isotopic signatures of stratospheric air at the himalayas and beyond, Sci. Bull., in press, https://doi.org/10.1016/j.scib.2020.11.005, 2020.

Liu, X., and Chen, B.: Climatic warming in the Tibetan Plateau during recent decades, Int. J. Climatol., 20, 1729-1742, https://doi.org/10.1002/1097-0088(20001130)20:14<1729::aid-joc556>3.0.co;2-y, 2000.

Lyons, J. R.: Transfer of mass-independent fractionation in ozone to other oxygen-containing radicals in the atmosphere, Geophys. Res. Lett., 28, 3231-3234, https://doi.org/10.1029/2000gl012791, 2001.

https://doi.org/10.5194/acp-2020-1279
Preprint. Discussion started: 12 January 2021

Ma, Y., Wang, Y., Zhong, L., Wu, R., Wang, S., and Li, M.: The characteristics of atmospheric turbulence and radiation energy transfer and the structure of atmospheric boundary layer over the northern slope area of Himalaya, J. Meteorolog. Soc. Jpn., 89, 345-353, https://doi.org/10.2151/jmsj.2011-a24, 2011.

Massling, A., Nielsen, I. E., Kristensen, D., Christensen, J. H., Sørensen, L. L., Jensen, B., Nguyen, Q., Nøjgaard, J. K., Glasius, M., and Skov, H.: Atmospheric black carbon and sulfate concentrations in Northeast Greenland, Atmos. Chem. Phys, 15, 9681-9692, https://doi.org/10.5194/acp-15-9681-2015, 2015.

McCabe, J. R., Savarino, J., Alexander, B., Gong, S., and Thiemens, M. H.: Isotopic constraints on non-photochemical sulfate production in the Arctic winter, Geophys. Res. Lett., 33, https://doi.org/10.1029/2005gl025164, 2006.

Mchenry, J. N., and Dennis, R. L.: The relative importance of oxidation pathways and clouds to atmospheric ambient sulfate production as predicted by the regional acid deposition model, J. Appl. Meteorol., 33, 890-905, https://doi.org/10.1175/1520-0450(1994)033<0890:trioop>2.0.co;2, 1994.

Michalski, G., Scott, Z., Kabiling, M., and Thiemens, M. H.: First measurements and modeling of $\Delta^{17}O$ in atmospheric nitrate, Geophys. Res. Lett., 30, 1870, https://doi.org/10.1029/2003gl017015, 2003.

Patris, N., Delmas, R., Legrand, M., De Angelis, M., Ferron, F. A., Stiévenard, M., and Jouzel, J.: First sulfur isotope measurements in central Greenland ice cores along the preindustrial and industrial periods, J. Geophys. Res. Atmos., 107, ACH 6-1-ACH 6-11, https://doi.org/10.1029/2001jd000672, 2002.

Paulot, F., Jacob, D. J., Pinder, R., Bash, J., Travis, K., and Henze, D.: Ammonia emissions in the United States, European Union, and China derived by high-resolution inversion of ammonium wet deposition data: Interpretation with a new agricultural emissions inventory (MASAGE_NH3), J. Geophys. Res. Atmos., 119, 4343-4364, https://doi.org/10.1002/2013jd021130, 2014.

Priyadarshi, A., Hill‐Falkenthal, J., Thiemens, M., Zhang, Z., Lin, M., Chan, C. y., and Kang, S.: Cosmogenic ^{35}S measurements in the Tibetan Plateau to quantify glacier snowmelt, J. Geophys. Res. Atmos., 119, 4125-4135, https://doi.org/10.1002/2013jd019801, 2014.

Prospero, J. M., Ginoux, P., Torres, O., Nicholson, S. E., and Gill, T. E.: Environmental characterization of global sources of atmospheric soil dust identified with the Nimbus 7 Total Ozone Mapping Spectrometer (TOMS) absorbing aerosol product, Rev. Geophys., 40, 2-1-2-31, https://doi.org/10.1029/2000rg000095, 2002.

Putero, D., Marinoni, A., Bonasoni, P., Calzolari, F., Rupakheti, M., and Cristofanelli, P.: Black carbon and ozone variability at the Kathmandu Valley and at the southern Himalayas: a comparison between a "hot spot" and a downwind high-altitude site, Aerosol Air Qual. Res., 18, 623-635+ ap621, https://doi.org/10.4209/aaqr.2017.04.0138, 2018.

Pye, H., Liao, H., Wu, S., Mickley, L. J., Jacob, D. J., Henze, D. K., and Seinfeld, J.: Effect of changes in climate and emissions on future sulfate-nitrate-ammonium aerosol levels in the United States, J. Geophys. Res. Atmos., 114, https://doi.org/10.1029/2008jd010701, 2009.

Pye, H. O., Nenes, A., Alexander, B., Ault, A. P., Barth, M. C., Clegg, S. L., Collett Jr, J. L., Fahey, K. M., Hennigan, C. J., and Herrmann, H.: The acidity of atmospheric particles and clouds, Atmos. Chem. Phys., 20, 4809-4888, https://doi.org/10.5194/acp-20-4809-2020, 2020.

Ram, K., Sarin, M., and Hegde, P.: Long-term record of aerosol optical properties and chemical composition from a high-altitude site (Manora Peak) in Central Himalaya, Atmos. Chem. Phys., 10, 11791, https://doi.org/10.5194/acp-10-11791-2010, 2010.

Ramanathan, V., Chung, C., Kim, D., Bettge, T., Buja, L., Kiehl, J., Washington, W., Fu, Q., Sikka, D., and Wild, M.: Atmospheric brown clouds: Impacts on South Asian climate and hydrological cycle, Proc. Natl. Acad. Sci. U.S.A., 102, 5326-5333, https://doi.org/10.1073/pnas.0500656102, 2005.

Savarino, J., and Thiemens, M. H.: Analytical procedure to determine both $\delta^{18}O$ and $\delta^{17}O$ of H_2O_2 in natural water and first measurements, Atmos. Environ., 33, 3683-3690, https://doi.org/10.1016/s1352-2310(99)00122-3, 1999.

Savarino, J., Lee, C. C., and Thiemens, M. H.: Laboratory oxygen isotopic study of sulfur (IV) oxidation: Origin of the mass-independent oxygen isotopic anomaly in atmospheric sulfates and sulfate mineral deposits on Earth, J. Geophys. Res. Atmos., 105, 29079-29088, https://doi.org/10.1029/2000jd900456, 2000.

Savarino, J., Alexander, B., Darmohusodo, V., and Thiemens, M. H.: Sulfur and oxygen isotope analysis of sulfate at micromole levels using a pyrolysis technique in a continuous flow system, Anal. Chem., 73, 4457-4462, https://doi.org/10.1021/ac010017f, 2001.

https://doi.org/10.5194/acp-2020-1279
Preprint. Discussion started: 12 January 2021

Savarino, J., Kaiser, J., Morin, S., Sigman, D. M., and Thiemens, M.: Nitrogen and oxygen isotopic constraints on the origin of atmospheric nitrate in coastal Antarctica, Atmos. Chem. Phys., 7, 1925-1945, https://doi.org/10.5194/acp-7-1925-2007, 2007.

Schauer, A. J., Kunasek, S. A., Sofen, E. D., Erbland, J., Savarino, J., Johnson, B. W., Amos, H. M., Shaheen, R., Abaunza, M., and Jackson, T. L.: Oxygen isotope exchange with quartz during pyrolysis of silver sulfate and silver nitrate, Rapid Commun. Mass Spectrom., 26, 2151-2157, https://doi.org/10.1002/rcm.6332, 2012.

Schwartz, S. E.: Aqueous-phase reactions in clouds, in: The Chemistry of Acid Rain: Sources and Atmospheric Processes, edited by: Johnson, R. W., and Gordon, G. E., ACS Publications, United States, 93-108, 1987.

Seinfeld, J. H., and Pandis, S. N.: Atmospheric chemistry and physics: from air pollution to climate change, edited by: Seinfeld, J., and Pandis, S., John Wiley & Sons, New York, 2016.

Shah, V., Jacob, D. J., Moch, J. M., Wang, X., and Zhai, S.: Global modeling of cloud water acidity, precipitation acidity, and acid inputs to ecosystems, Atmos. Chem. Phys., 20, 12223-12245, https://doi.org/10.5194/acp-20-12223-2020, 2020.

Sherwen, T., Schmidt, J. A., Evans, M. J., Carpenter, L. J., Großmann, K., Eastham, S. D., Jacob, D. J., Dix, B., Koenig, T. K., and Sinreich, R.: Global impacts of tropospheric halogens (Cl, Br, I) on oxidants and composition in GEOS-Chem, Atmos. Chem. Phys., 16, 12239-12271, https://doi.org/10.5194/acp-16-12239-2016, 2016.

Škerlak, B., Sprenger, M., and Wernli, H.: A global climatology of stratosphere-troposphere exchange using the ERA-Interim data set from 1979 to 2011, Atmos. Chem. Phys., 14, 913-937, https://doi.org/10.5194/acp-14-913-2014, 2014.

Sofen, E., Alexander, B., and Kunasek, S.: The impact of anthropogenic emissions on atmospheric sulfate production pathways, oxidants, and ice core $\Delta^{17}O(SO_4^{2-})$, Atmos. Chem. Phys., 11, 3565-3578, https://doi.org/10.5194/acp-11-3565-2011, 2011.

Stein, A., Draxler, R. R., Rolph, G. D., Stunder, B. J., Cohen, M., and Ngan, F.: NOAA's HYSPLIT atmospheric transport and dispersion modeling system, Bull. Am. Meteorol. Soc., 96, 2059-2077, https://doi.org/10.1175/bams-d-14-00110.1, 2015.

Stockwell, W. R., and Calvert, J. G.: The mechanism of the HO-SO_2 reaction, Atmos. Environ., 17, 2231-2235, https://doi.org/10.1016/0004-6981(83)90220-2, 1983.

Thiemens, M. H., and Heidenreich, J. E.: The mass-independent fractionation of oxygen: A novel isotope effect and its possible cosmochemical implications, Science, 219, 1073-1075, https://doi.org/10.1126/science.219.4588.1073, 1983.

Thiemens, M. H.: Mass-independent isotope effects in planetary atmospheres and the early solar system, Science, 283, 341-345, https://doi.org/10.1126/science.283.5400.341, 1999.

Turnock, S., Mann, G., Woodhouse, M., Dalvi, M., O'Connor, F., Carslaw, K., and Spracklen, D.: The impact of changes in cloud water pH on aerosol radiative forcing, Geophys. Res. Lett., 46, 4039-4048, https://doi.org/10.1029/2019gl082067, 2019.

Ullerstam, M., Vogt, R., Langer, S., and Ljungström, E.: The kinetics and mechanism of SO_2 oxidation by O_3 on mineral dust, Phys. Chem. Chem. Phys., 4, 4694-4699, https://doi.org/10.1039/b203529b, 2002.

Van Marle, M. J., Kloster, S., Magi, B. I., Marlon, J. R., Daniau, A.-L., Field, R. D., Arneth, A., Forrest, M., Hantson, S., and Kehrwald, N. M.: Historic global biomass burning emissions based on merging satellite observations with proxies and fire models (1750-2015), Geosci. Model Dev., 10, 3329-3357, https://doi.org/10.5194/gmd-10-3329-2017, 2017.

Vicars, W. C., and Savarino, J.: Quantitative constraints on the ^{17}O-excess ($\Delta^{17}O$) signature of surface ozone: Ambient measurements from 50 N to 50 S using the nitrite-coated filter technique, Geochim. Cosmochim. Acta, 135, 270-287, https://doi.org/10.1016/j.gca.2014.03.023, 2014.

Vogt, R., Crutzen, P. J., and Sander, R.: A mechanism for halogen release from sea-salt aerosol in the remote marine boundary layer, Nature, 383, 327-330, https://doi.org/10.1038/383327a0, 1996.

Walters, W. W., Michalski, G., Böhlke, J. K., Alexander, B., Savarino, J., and Thiemens, M. H.: Assessing the seasonal dynamics of nitrate and sulfate aerosols at the South Pole utilizing stable isotopes, J. Geophys. Res. Atmos., 124, 8161-8177, https://doi.org/10.1029/2019jd030517, 2019.

Wang, K., Hattori, S., Kang, S., Lin, M., and Yoshida, N.: Isotopic constraints on the formation pathways and sources of atmospheric nitrate in the Mt. Everest region, Environ. Pollut., 115274, https://doi.org/10.1016/j.envpol.2020.115274, 2020a.

Wang, R., Tao, S., Balkanski, Y., Ciais, P., Boucher, O., Liu, J., Piao, S., Shen, H., Vuolo, M. R., and Valari, M.: Exposure to ambient black carbon derived from a unique inventory and high-resolution model, Proc. Natl. Acad. Sci. U.S.A., 111, 2459-2463, https://doi.org/10.1073/pnas.1318763111, 2014.

https://doi.org/10.5194/acp-2020-1279
Preprint. Discussion started: 12 January 2021

Atmospheric Chemistry and Physics Discussions

Wang, T., Tang, J., Sun, M., Liu, X., Huang, Y., Huang, J., Han, Y., Cheng, Y., Huang, Z., and Li, J.: Identifying a transport mechanism of dust aerosols over South Asia to the Tibetan Plateau: A case study, Sci. Total Environ., 143714, https://doi.org/10.1016/j.scitotenv.2020.143714, 2020b.

Wang, W., Xu, W., Collett Jr, J. L., Liu, D., Zheng, A., Dore, A. J., and Liu, X.: Chemical compositions of fog and precipitation at Sejila Mountain in the southeast Tibetan Plateau, China, Environ. Pollut., 253, 560-568, https://doi.org/10.1016/j.envpol.2019.07.055, 2019a.

Wang, Y., Zhang, X., and Draxler, R. R.: TrajStat: GIS-based software that uses various trajectory statistical analysis methods to identify potential sources from long-term air pollution measurement data, Environ. Modell. Ssoftw, 24, 938-939, https://doi.org/10.1016/j.envsoft.2009.01.004, 2009.

Wang, Y. L., Song, W., Yang, W., Sun, X. C., Tong, Y. D., Wang, X. M., Liu, C. Q., Bai, Z. P., and Liu, X. Y.: Influences of atmospheric pollution on the contributions of major oxidation pathways to PM2. 5 nitrate formation in Beijing, J. Geophys. Res. Atmos., 124, 4174-4185, https://doi.org/10.1029/2019jd030284, 2019b.

Xia, X., Zong, X., Cong, Z., Chen, H., Kang, S., and Wang, P.: Baseline continental aerosol over the central Tibetan plateau and a case study of aerosol transport from South Asia, Atmos. Environ., 45, 7370-7378, https://doi.org/10.1016/j.atmosenv.2011.07.067, 2011.

Xie, L., Spiro, B., and Wei, G.: Purification of $BaSO_4$ precipitate contaminated with organic matter for oxygen isotope measurements ($\delta^{18}O$ and $\Delta^{17}O$), Rapid Commun. Mass Spectrom., 30, 1727-1733, https://doi.org/10.1002/rcm.7610, 2016.

Yang, Y., Zhou, R., Yan, Y., Yu, Y., Liu, J., Du, Z., and Wu, D.: Seasonal variations and size distributions of water-soluble ions of atmospheric particulate matter at Shigatse, Tibetan Plateau, Chemosphere, 145, 560-567, https://doi.org/10.1016/j.chemosphere.2015.11.065, 2016.

Yin, X., Kang, S., de Foy, B., Cong, Z., Luo, J., Zhang, L., Ma, Y., Zhang, G., Rupakheti, D., and Zhang, Q.: Surface ozone at Nam Co in the inland Tibetan Plateau: variation, synthesis comparison and regional representativeness, Atmos. Chem. Phys., 17, https://doi.org/10.5194/acp-17-11293-2017, 2017.

Yuen, P.-F., Hegg, D. A., Larson, T. V., and Barth, M. C.: Parameterization of heterogeneous droplet chemistry for use in bulk cloud models, J. Appl. Meteorol., 35, 679-689, https://doi.org/10.1175/1520-0450(1996)035<0679:POHDCF>2.0.CO;2, 1996.

Zheng, X., Shen, C., Wan, G., Liu, K., Tang, J., and Xu, X.: $^{10}Be/^{7}Be$ implies the contribution of stratosphere-troposphere transport to the winter-spring surface O_3 variation observed on the Tibetan Plateau, Chin. Sci. Bull., 56, 84-88, https://doi.org/10.1007/s11434-010-4211-3, 2011.

https://doi.org/10.5194/acp-2020-1279
Preprint. Discussion started: 12 January 2021

Atmospheric Chemistry and Physics Discussions

Table 1 Concentrations and $\Delta^{17}O$ values of atmospheric sulfate collected in the Mt. Everest region for individual sampling durations as well as the corresponding meteorological parameters including relative humidity (RH) and temperature. The relative contribution of SO_2 oxidation by O_3 to SAS for each sample is also shown as $f_{O3,\,min}$ and $f_{O3,\,max}$.

Seasons	Samples	Sampling period	[bulk-SO_4^{2-}] (nmol/m^3)	[nd-SO_4^{2-}] (nmol/m^3)	$\Delta^{17}O(SO_4^{2-})_{bulk}$ (‰)	$\Delta^{17}O(SO_4^{2-})_{SAS}$ (‰)	$f_{O3,\,min}$ (%)	$f_{O3,\,max}$ (%)	RH (%)	Temp. (°C)
Pre-monsoon (n = 13)	1	Apr. 10-Apr. 14	8.47	8.14	1.6 ± 0.1	1.7 ± 0.1	16 ± 4	26 ± 3	44.52	3.57
	2	Apr. 14-Apr. 18	21.26	20.29	1.7 ± 0.1	1.7 ± 0.1	16 ± 4	27 ± 3	48.30	3.10
	3	Apr. 18-Apr. 22	16.50	15.88	1.7 ± 0.1	1.7 ± 0.1	17 ± 4	27 ± 3	37.77	4.81
	4	Apr. 22-Apr. 25	24.61	23.32	1.3 ± 0.1	1.3 ± 0.1	9 ± 4	21 ± 2	40.02	3.32
	5	Apr. 25-Apr. 28	14.50	13.72	1.6 ± 0.1	1.7 ± 0.1	15 ± 4	26 ± 3	47.72	2.56
	6	Apr. 28-May. 1	11.93	11.17	0.6 ± 0.1	0.6 ± 0.1	0	10 ± 2	61.73	2.40
	7	May. 1-May. 5	14.32	13.24	1.6 ± 0.1	1.7 ± 0.1	16 ± 4	26 ± 3	42.82	4.90
	8	May. 5-May. 13	15.11	14.41	0.7 ± 0.1	0.8 ± 0.1	0	12 ± 2	32.76	5.97
	9	May. 13-May. 17	9.86	9.17	1.6 ± 0.1	1.7 ± 0.1	17 ± 4	27 ± 3	48.78	6.11
	10	May. 17-May. 21	5.11	4.84	1.6 ± 0.1	1.7 ± 0.1	15 ± 4	26 ± 3	47.14	8.04
	11	May. 21-May. 25	5.85	5.47	1.6 ± 0.1	1.7 ± 0.1	16 ± 4	26 ± 3	42.77	10.48
	12	May. 25-May. 29	24.10	23.15	0.8 ± 0.1	0.9 ± 0.1	1 ± 4	13 ± 2	43.67	8.41
	13	May. 29-Jun. 2	20.44	19.68	0.5 ± 0.1	0.5 ± 0.1	0	7 ± 2	49.48	8.23
					Average	1.4 ± 0.5				
					Weighted average	1.2 ± 0.6				
Monsoon (n = 11)	14	Jun. 2-Jun. 6	6.56	6.37	1.2 ± 0.1	1.3 ± 0.1	8 ± 4	19 ± 2	57.62	8.27
	15	Jun. 8-Jun. 9	15.92	15.48	1.3 ± 0.1	1.3 ± 0.1	9 ± 4	21 ± 2	59.47	10.70
	16	Jun. 9-Jun. 15	3.44	3.30	2.1 ± 0.1	2.2 ± 0.2	25 ± 5	34 ± 3	52.17	11.69
	17	Jun. 15-Jun. 20	5.10	4.86	2.9 ± 0.1	3.0 ± 0.2	39 ± 6	47 ± 4	47.20	11.62
	18	Jun. 20-Jun. 29	5.32	5.13	1.7 ± 0.1	1.7 ± 0.1	16 ± 4	26 ± 3	50.92	12.41
	19	Jul. 7-Jul. 17	1.30	1.23	2.0 ± 0.1	2.1 ± 0.2	22 ± 5	32 ± 3	71.10	11.12
	20	Jul. 17-Jul. 28	1.11	1.01	1.9 ± 0.1	2.1 ± 0.2	23 ± 5	33 ± 3	70.08	10.86
	21	Jul. 28-Aug. 1	1.48	1.34	2.0 ± 0.1	2.2 ± 0.2	25 ± 5	34 ± 3	66.73	11.11
	22	Aug. 1-Aug. 11	1.52	1.33	1.6 ± 0.1	1.8 ± 0.2	18 ± 5	28 ± 3	73.74	10.02
	23	Aug. 11-Aug. 17	1.40	1.27	1.8 ± 0.1	2.0 ± 0.2	22 ± 5	31 ± 3	68.45	10.95
	24	Jul. 17-Sep. 1	1.37	1.17	1.7 ± 0.1	2.0 ± 0.2	21 ± 5	31 ± 3	68.70	11.01
					Average	2.0 ± 0.5				
					Weighted average	1.9 ± 0.7				
Post-monsoon (n = 2)	25	Sep. 1-Sep. 10	2.79	2.49	1.4 ± 0.1	1.6 ± 0.1	14 ± 4	24 ± 3	54.86	11.97
	26	Sep. 11-Sep. 21	4.58	4.33	1.7 ± 0.1	1.8 ± 0.1	17 ± 4	27 ± 3	53.38	9.49

745

https://doi.org/10.5194/acp-2020-1279
Preprint. Discussion started: 12 January 2021

Atmospheric Chemistry and Physics Discussions

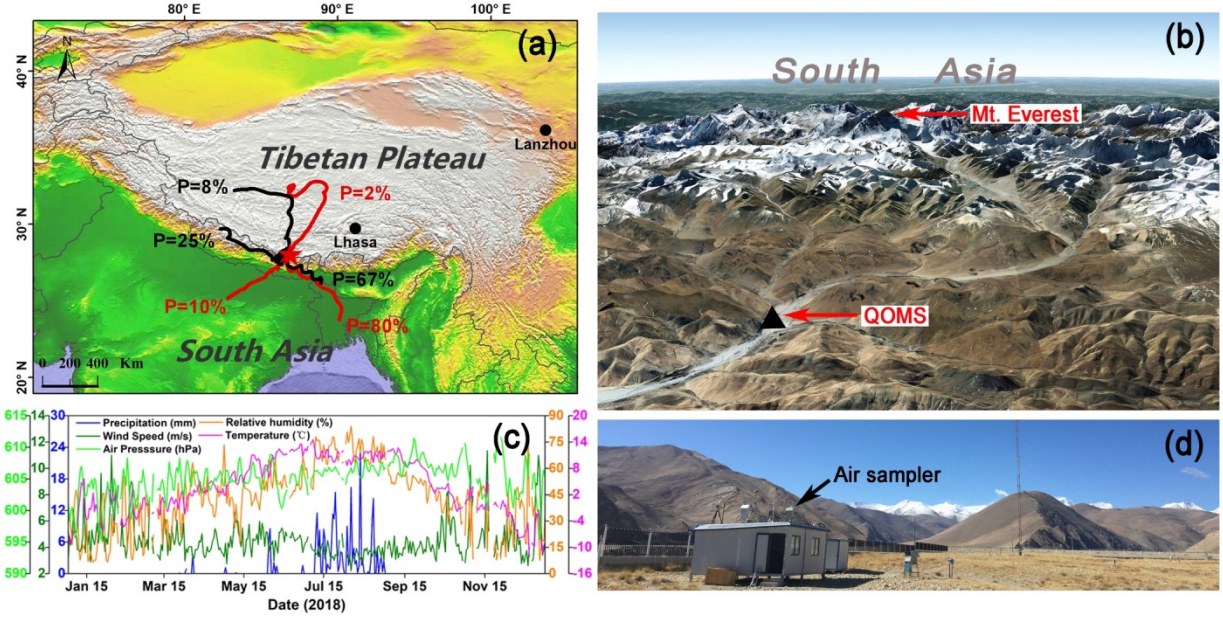

Figure 1: (a) A map showing the geographic location of the sampling site (QOMS, red star) with clustered five-day backward trajectories of air masses arriving at QOMS during different seasons in 2018 (black lines stand for pre-monsoon and red lines stand for monsoon; the clusters were shown with respective percentage (P) of trajectories); (b) detailed terrain features around the QOMS and Mt. Everest (image from © Google Earth); (c) seasonal variations of meteorological parameters measured at the QOMS, and (d) a picture showing the sampling site and surroundings.

https://doi.org/10.5194/acp-2020-1279
Preprint. Discussion started: 12 January 2021

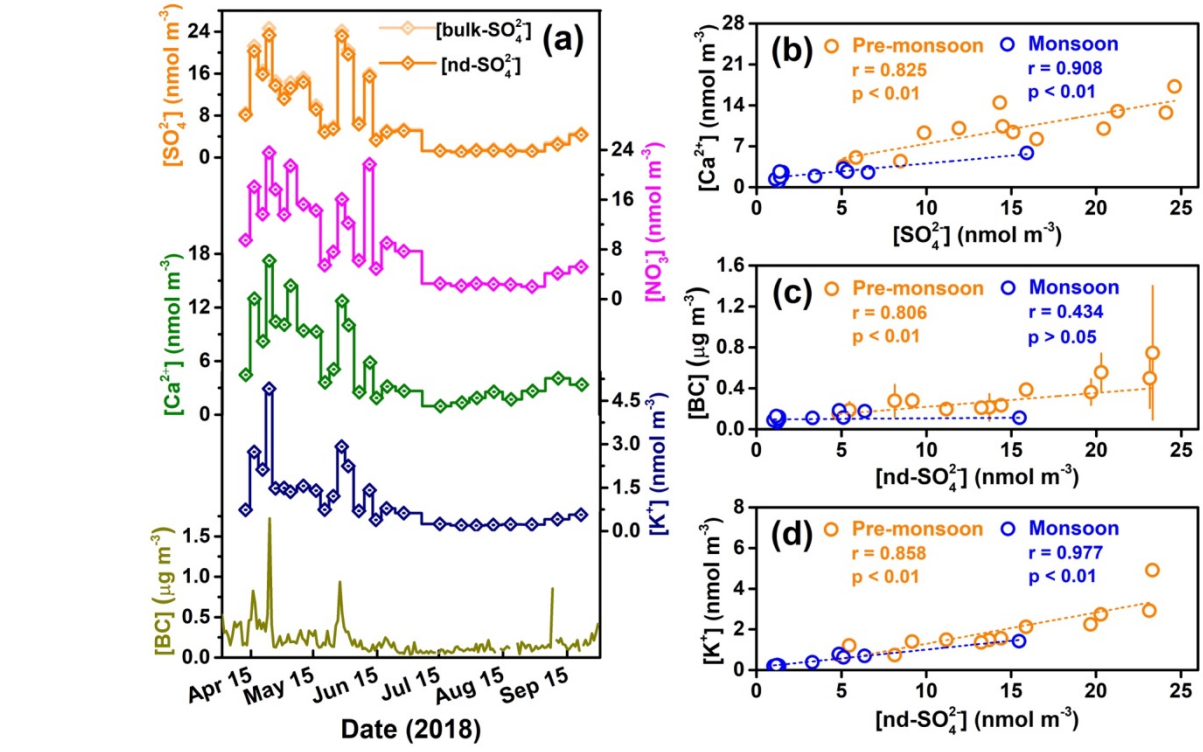

Figure 2: (a) Temporal variations in concentrations of major ions in TSP samples collected from the Mt. Everest region across the entire study period, and (b-d) correlations between [bulk-SO_4^{2-}] and [Ca^{2+}], [nd-SO_4^{2-}] and [BC], as well as [nd-SO_4^{2-}] and [K^+] in the pre-monsoon and monsoon seasons. The error bars in Fig. 2(c) stand for 1σ-uncertainty.

https://doi.org/10.5194/acp-2020-1279
Preprint. Discussion started: 12 January 2021

Atmospheric Chemistry and Physics Discussions

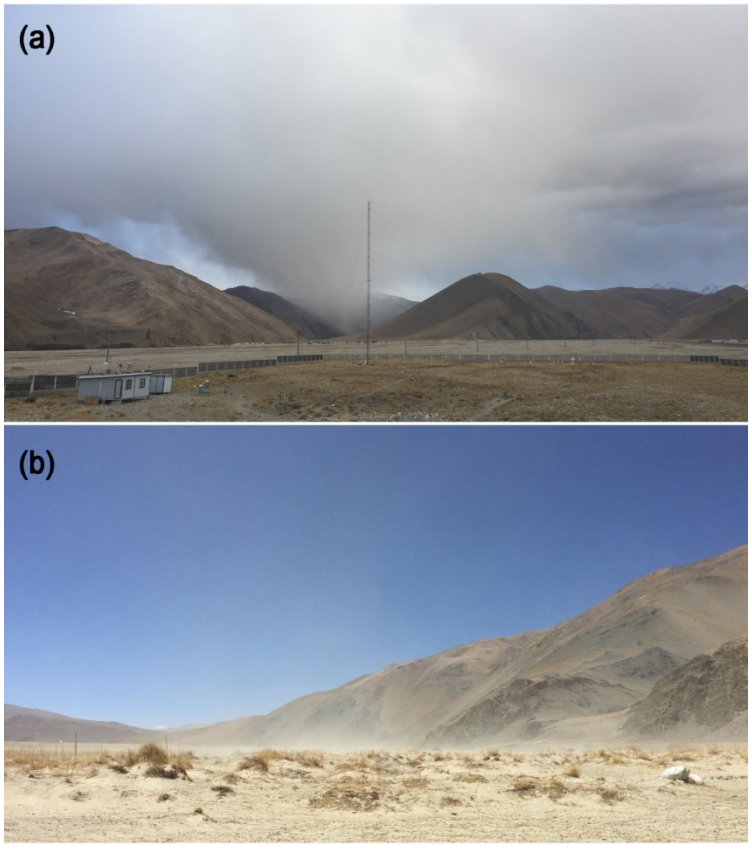

Figure 3: Pictures of a dust storm (a) as well as the re-suspended dust (b) in the Mt. Everest region.

https://doi.org/10.5194/acp-2020-1279
Preprint. Discussion started: 12 January 2021

Atmospheric Chemistry and Physics Discussions

760

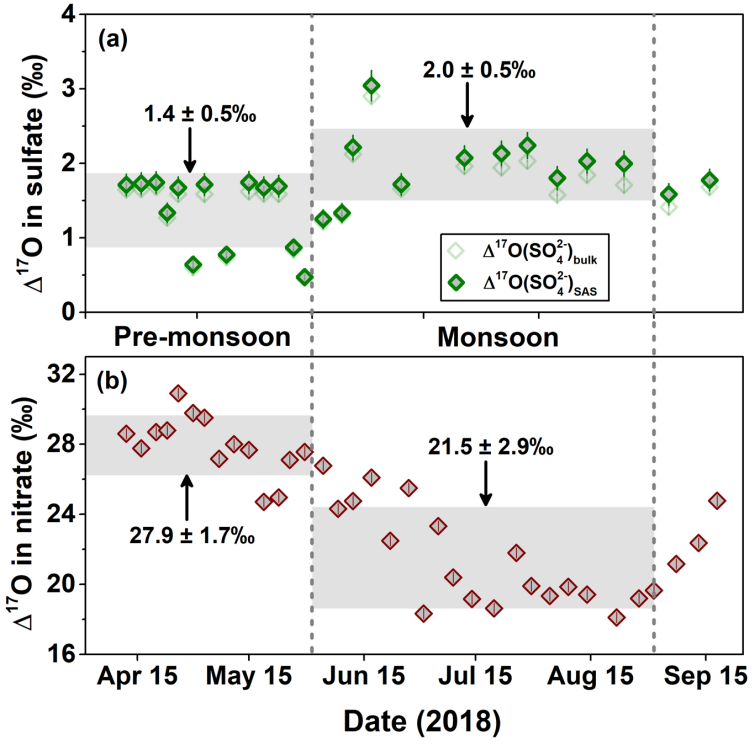

Figure 4: Seasonal changes in (a) $\Delta^{17}O(SO_4^{2-})_{bulk}$ and $\Delta^{17}O(SO_4^{2-})_{SAS}$ (this study) and (b) $\Delta^{17}O(NO_3^-)$ in in the Mt. Everest region (Wang et al., 2020a). The light grey horizontal bands are the seasonal average of $\Delta^{17}O$ with 1σ-uncertainty. For $\Delta^{17}O(SO_4^{2-})_{bulk}$ and $\Delta^{17}O(NO_3^-)$, the error bars are analytical uncertainties, while for $\Delta^{17}O(SO_4^{2-})_{SAS}$, the error bars stand for the propagated analytical uncertainties.

765

https://doi.org/10.5194/acp-2020-1279
Preprint. Discussion started: 12 January 2021

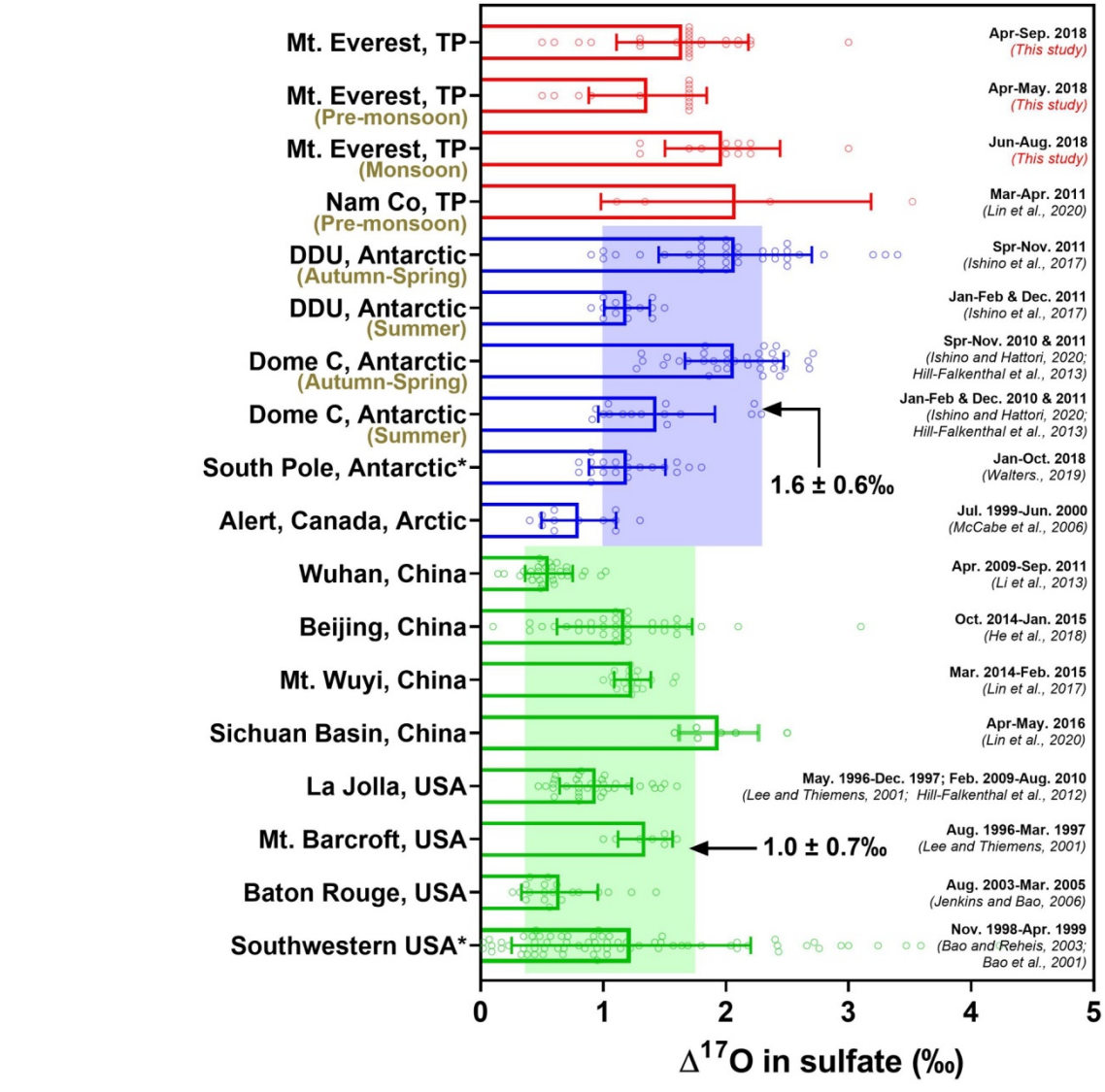

Figure 5: Compilation of $\Delta^{17}O$ in modern atmospheric sulfate observed at diverse geographic localities to date, including the TP region (red), polar regions (blue), and other mid-latitude regions (green). $\Delta^{17}O(SO_4^{2-})$ values were averaged with 1σ-uncertainty. Asterisk (*) represents $\Delta^{17}O$ values measured from bulk atmospheric sulfate, which will bias these $\Delta^{17}O$ observations low; the remaining stand for $\Delta^{17}O$ values in SAS.

https://doi.org/10.5194/acp-2020-1279
Preprint. Discussion started: 12 January 2021

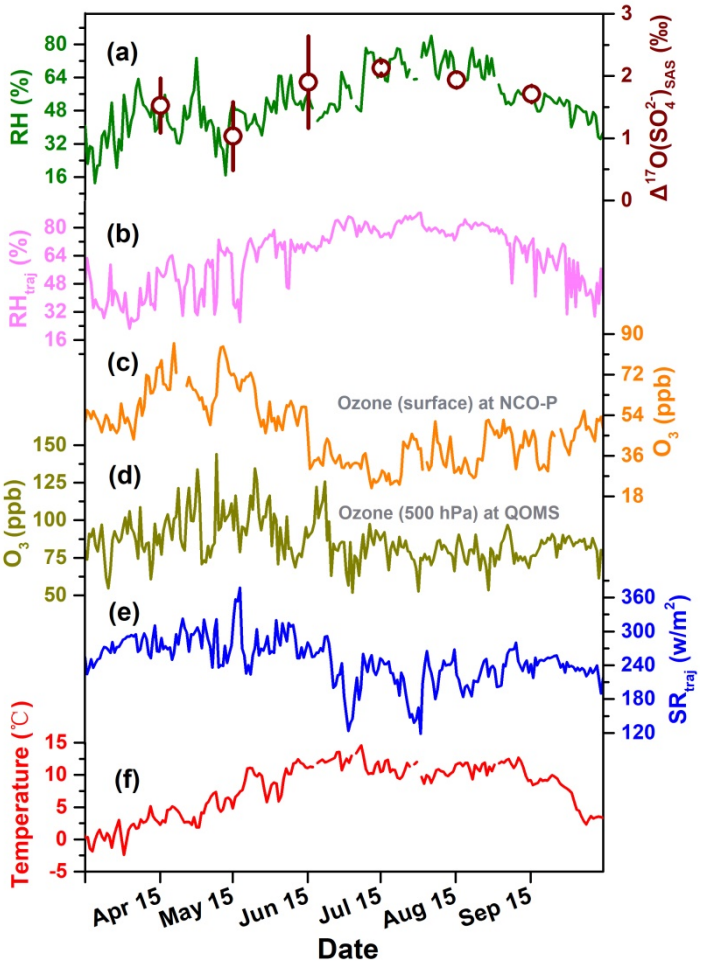

Figure 6: Seasonal patterns of (a) relative humidity (RH) and monthly weighted average values of $\Delta^{17}O(SO_4^{2-})_{SAS}$ with 1σ-uncertainty, (b) relative humidity along with backward trajectories arriving at the sampling sites (RH_{traj}), (c) ozone mixing ratio at surface level at NCO-P from Putero et al. (2018), (d) ozone mixing ratio at 500 hPa at QOMS, (e) solar radiation fluxes along with backward trajectories arriving at the sampling sites (SR_{traj}), and (f) temperature.

https://doi.org/10.5194/acp-2020-1279
Preprint. Discussion started: 12 January 2021

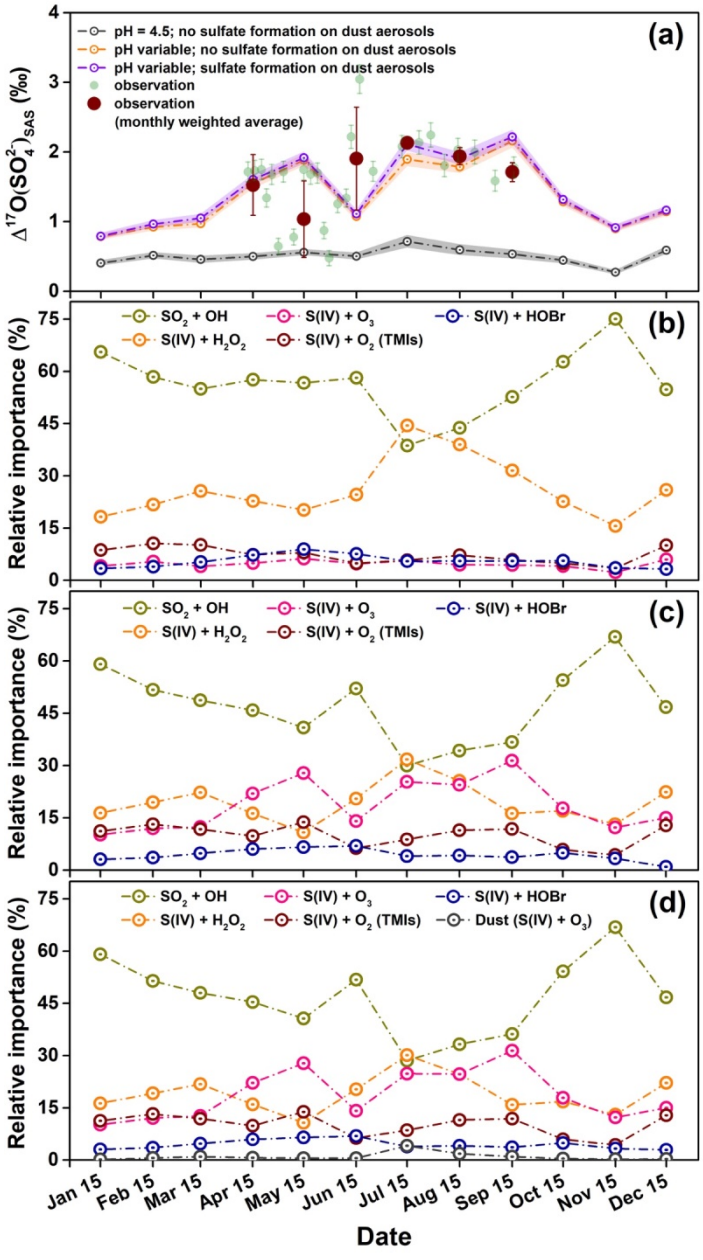

Figure 7: (a) Comparison of modeled and observed $\Delta^{17}O(SO_4^{2-})_{SAS}$ at the Mt. Everest region. The shaded area for the modeled $\Delta^{17}O(SO_4^{2-})$ indicates the 1σ-uncertainty. (b-d) Modeled relative fraction of sulfate formation pathways under the conditions of (b) cloud water pH = 4.5 and no sulfate formation on dust aerosols, (c) variable cloud water pH and no sulfate formation on dust aerosols, and (d) variable cloud water pH and considering the sulfate formation on dust aerosols.

https://doi.org/10.5194/acp-2020-1279
Preprint. Discussion started: 12 January 2021

Atmospheric Chemistry and Physics Discussions

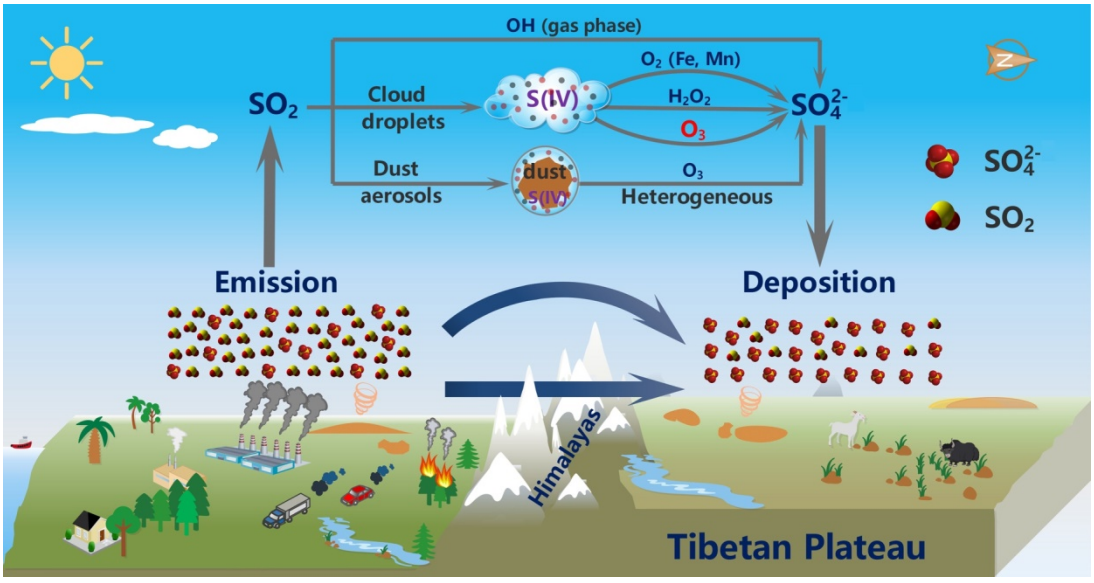

785

Figure 8: Schematic illustration of South Asia sourced sulfate aerosols as well as its formation mechanism in the troposphere during the long-range cross-border transport over the Himalayas, which contribute significantly to the sulfate levels in the Mt. Everest region, and even the entire southern TP.